

## Effect of electrical operating conditions on thermal behavior of PV modules: Numerical and experimental analysis



Amr Osama <sup>a,b,c</sup> , Giuseppe Marco Tina <sup>a,\*</sup> , Antonio Gagliano <sup>a</sup> ,  
Gabino Jimenez-Castillo <sup>d</sup> , Francisco José Munoz-Rodríguez <sup>e</sup>

<sup>a</sup> University of Catania, Department of Electric, Electronics and Computer Engineering, Viale Andrea Doria 6, Catania, 95125, Italy

<sup>b</sup> Department of Information and Electrical Engineering and Applied Mathematics (DIEM) – University of Salerno (UNISA), Via Giovanni Paolo II, 132, Fisciano 84084, SA, Italy

<sup>c</sup> Mechanical Power Engineering Department, Faculty of Engineering, Port Said University, Port Fuad, Egypt

<sup>d</sup> Department of Electrical Engineering, Center for Advanced Studies in Earth Sciences, Energy and Environment, University of Jaén, Jaén, Spain

<sup>e</sup> Department of Electronic and Automatic Engineering, Universidad de Jaén, Jaén, 23071, Spain

### ARTICLE INFO

#### Keywords:

Thermal model  
Temperature  
Short circuit  
Open circuit  
Maximum power point  
Performance

### ABSTRACT

The rapid growth of photovoltaic (PV) energy has the potential to transform the global energy landscape. However, the intermittent nature of solar power presents significant challenges to grid integration, such as overgeneration and curtailment. Consequently, PV systems may operate at points other than the maximum power point (MPP). Monitoring the thermal behavior of photovoltaic systems is critical due to its impact on productivity and system health. Most studies focus on meteorological variables, often overlooking the influence of electrical operating states on thermal performance. Thus the objective is to evaluate the accuracy of existing thermal models from the literature and widely used specialized software tools—alongside their commonly cited coefficients against different electrical operating status (EOS). This study investigates the thermal behavior of PV modules under different EOS: short-circuited (PVset-1), open-circuited (PVset-2), and operating at MPP (PVset-3). The experiment was conducted over four months at Jaén University campus in Spain. Results showed the short-circuited module's temperature was 6.90 °C higher, and the open-circuited module's temperature was 3.67 °C higher than the MPP module. Thermographic investigations revealed multiple hotspots in the short-circuited set. These hotspots can severely impact the module's long-term reliability and efficiency. The analysis of thermal models considering these operating states indicated an overestimation of the MPP module's temperature. However, the Keddouda model demonstrated high accuracy potential, with an average deviation of less than 3.4 %, particularly at high irradiance levels. These findings highlight the necessity of considering EOS in thermal models to enhance the accuracy and reliability of PV system performance assessments.

### 1. Introduction

Nowadays, many countries have set ambitious goals to reduce their CO<sub>2</sub> emissions, driving the electricity sector toward an unprecedented deployment of renewable energy. [1,2]. In 2018–2023, the worldwide renewable installed capacity has grown by 61 % [3], but photovoltaic has provided the largest contribution, growing from 0.52 TW in 2018 to 1.6 TW in 2023 [4]. The exponential growth of photovoltaic installed capacity has also been driven by a significant technology cost reduction, in particular in terms of capital costs and so of levelized cost of energy that, according to Ref. [5] in 2023 is 0.044 \$/kWh that –90 % respect

2010.

As the penetration of variable renewable energy (VRE) increases, the share of curtailed wind and solar PV generation is also on the rise in many markets. This trend is particularly evident in areas where major grid infrastructure investments and/or advanced market design and regulation are not keeping pace with VRE deployment [3]. Although VRE curtailment is increasing overall, the share of curtailed wind and solar PV generation remains relatively low, ranging from 1.5 % to 4 % in most large renewable energy markets. However, higher VRE shares do not necessarily result in rising curtailment rates, as countries can effectively manage renewable energy integration challenges with timely

\* Corresponding author.

E-mail address: [giuseppe.tina@unict.it](mailto:giuseppe.tina@unict.it) (G.M. Tina).

measures [3]. One such solution is the forecasting of PV production and load, as predicting events in advance facilitates better management and reduces curtailment risks.

The photovoltaics module is the key component producing electrical energy that requires continuous monitoring for system reliability. A better understanding of the key factors that have a great influence on the PV module performance is essential specifically for performance evaluation and prediction. The temperature of a PV module plays a vital role in determining its efficiency, longevity, and overall performance. As module temperatures rise, solar cells experience a decline in efficiency due to the negative temperature coefficient, causing a reduction in power output—typically around 0.4%–0.5% per degree Celsius above 25 °C, depending on the PV module technology and material. This effect is particularly noticeable in warm climates, where high temperatures can lead to significant energy losses. Beyond efficiency, excessive heat can cause thermal stress, leading to material degradation, microcracks, and potential long-term damage to the module [6]. Moreover, continuous experiencing high module temperature can lead to irreversible faults, reducing the module efficiency and shortening the lifetime of the module [7,8]. Thus, monitoring temperature is essential for early fault detection, as overheating can lead to issues like hot spots, which may permanently damage the module. By understanding and managing PV module temperature, solar energy systems can be optimized for higher efficiency, better reliability, and longer service life.

To monitor the instant temperature of the PV system, temperature sensors are fixed at the rear side of the operating PV module, recording the real-time measurement of the module temperature ( $T_m$ ), which can be compared to the thermal model as a reference that predicts the module temperature if it operates in the same environmental variables [9]. Thermal modeling of PV modules is essential for predicting temperature behavior, optimizing energy output, and ensuring long-term reliability. Thermal modeling can also be used to assess cooling strategies. Integrating thermal modeling into PV analysis, aids in fault detection and helps prevent issues like hot spots that could damage the module.

In addition to the data-driven modeling [10,11] and numerical modeling methods [12,13], there are two dominant thermal modeling approaches for predicting module temperature: dynamic models and steady-state thermal models depending on the research purposes or the software tools employed [14]. Dynamic models [15,16] include the thermal response of the module, which implies the thermal transient response of the PV modules. Dynamic models depend on the energy balance between the PV module and the surrounding environment and consider weather variables, thermal capacity, heat transfer mechanisms (conduction, convection, and radiation), and electrical power conversion [17]. This enables the thermal investigation of the multilayers of the PV module to have better analysis and insight into the PV module's behavior with the surrounding environment [18]. These sophisticated models need significant computing time, money, and effort, yet they are preferred if the PV system output is modeled for high-resolution input data [19]. Based on the Finite Difference approach, a dynamic thermal model for the solar module was suggested. The Particle Swarm Optimization approach was used to optimize the model coefficients. The results confirmed the effectiveness of the suggested dynamic thermal model, with a temperature estimation error of no more than 9 °C [20].

The steady-state thermal models used for estimating PV module temperature usually neglect the module's thermal mass, assuming an instantaneous response of the module temperature to changing radiation [21]. These models are based on simplified heat transfer equations with empirically determined parameters [22] or entirely empirical equations [23]. Steady-state models are generally simple and have short processing durations, yet they can't accurately calculate the module temperature. Several thermal models, such as the Sandia, Nominal Operating Cell Temperature (NOCT), and Faiman models, are widely used to estimate PV module temperatures under varying environmental conditions. These models typically correlate plane-of-array irradiance (G<sub>POA</sub>),

ambient temperature ( $T_a$ ), and, in some cases, wind speed ( $\omega$ ) [24].

The NOCT model was first developed in the 1970s as part of efforts to standardize photovoltaic (PV) module temperature estimation [25], while the Sandia thermal model has been continuously developed by Sandia National Laboratories since 2004 [26]. The Faiman model, developed in 2008, has been incorporated into PVsyst [27], whereas the Duffie and Beckman thermal models, developed in 1990, are used in SAM [28]. These models and their empirical coefficients were developed approximately 20 years ago when the electrical efficiency of the studied PV modules was significantly lower than today. With recent advancements, module efficiency has increased to up to 25%, depending on the adopted technology [29–31]. Several literature reviews [19] have provided comprehensive overviews of these steady-state thermal models, highlighting the improvements made over the last decade and reinforcing their significance. Validation studies often involve comparing the model temperature prediction with experimental temperature data collected from field-installed PV systems, assessing the sensitivity of thermal models to environmental parameters [32]. For instance, wind speed significantly affects convective cooling, yet many models assume uniform wind profiles or neglect it, such as the NOCT model and Ross model, leading to discrepancies in transient conditions [33].

Servant [34] introduced a simplified linear model for estimating PV cell temperature in 1985. By applying the least squares method, the study determined coefficients linking module temperature to meteorological parameters with an observed error of around 4 °C. Mattei et al. [35] proposed a thermal model based on energy balance, incorporating a transmittance-absorptance coefficient ( $\tau\alpha = 0.81$ ) and an experimentally derived heat transfer coefficient, achieving a Mean Squared Error (MSE) of 2.24 °C. Mondol et al. [36] developed a temperature prediction model using measured ambient and module temperatures along with solar radiation, demonstrating improved accuracy compared to the NOCT approach. Pereira et al. [37] evaluated eight thermal models for predicting PV module temperature and power output, comparing their performance against measured backside temperatures. The Mattei steady-state model demonstrated the highest accuracy for temperature estimation (MBE = 0.4 °C, RMSE = 2.7 °C). For power output prediction, the Kurtz (Sandia1) model, combined with a single diode and 5 parameters model, outperformed others (MBE = 4.6 W, RMSE = 54.5 W). Several investigations focused on assessing the NOCT model [25,38], Sandia model [39], Skoplaki model [40] and other different thermal models, which confirms that such steady-state thermal models neglect the electrical operating status or even deal with the PV module as a flat plate solar collector [19]. Akhsassi et al. [41] validated 10 thermal models using experimental data based on ambient temperature and in-plane irradiance, with and without considering wind speed. Among models without wind, his model achieved the highest correlation ( $R^2 = 96.7\%$ ) and the lowest RMSE (1.6 °C). When accounting for wind, his model outperformed all others, achieving the best statistical performance with  $R^2 = 98.8\%$  and RMSE = 1.1 °C.

Apart from physical thermal modeling, recent advancements in data-driven thermal modeling using Machine Learning (ML) and artificial intelligence have shown great potential [42]. Different algorithms have been investigated and compared with usual physical models, especially for new installation configurations and PV technologies [43]. Keddouda et al. [42] examined 12 different ML and regression algorithms to evaluate their accuracy in predicting module temperature. The results showed that for linear modeling, the LASSO algorithm provided the best performance. However, the ANN model demonstrated the best overall results, achieving an  $R^2$  value of 0.986, an MAE of 0.982 °C, and an MSE of 2.181. Following up on this investigation, A new thermal model for free-standing photovoltaic modules has been developed [44], incorporating heat transfer principles and energy balance. The proposed simulation algorithm demonstrated strong performance, achieving an  $R^2$  of 0.963 and an MAE of 1.883 °C, closely matching King's model ( $R^2 = 0.973$ , MAE = 1.663 °C).

Despite the promising advancements in machine learning for PV

thermal modeling, several challenges remain in integrating ML with traditional physical models. A primary issue is the limited adaptability of ML models to diverse climatic conditions and PV system designs, largely due to their dependence on the quality and variety of available training data [45]. Furthermore, ML techniques often suffer from substantial computational demands and opaque decision-making processes, which hinder their interpretability and complicate the derivation of practical thermal parameters [46]. Recent studies have attempted to develop hybrid models that combine physics-based equations with ML techniques, but striking a balance between computational efficiency and physical accuracy remains an open research question [47,48].

The development of new PV technologies and installation configurations, such as floating PV systems, building integrated systems, and agrivoltaics, highlights the need for updated thermal models that can adapt to these advancements. The adoption of physical thermal models with specific configurations gained attention, especially because of their usage in the simulation software tools [49]. Several research have developed new coefficients to optimize the coefficients of the Faiman model for different floating configurations for both monofacial and bifacial PV modules [50,51]. Thermal modeling of the vertical east/west oriented bifacial PV module installed in Norway over a rooftop reported a constant thermal coefficient of  $55 \text{ W/m}^2\text{C}$  in the form of the Faiman model [52]. A similar setup analysis in the Netherlands reached a similar value of the thermal coefficient of  $56 \text{ W/m}^2\text{C}$  [53]. Moreover, the thermal performance of the Building Integrated Photovoltaic is studied and thoroughly investigated, yet the physical thermal modeling of vertical installation application didn't get enough consideration in the literature [54].

However, for emerging PV configurations such as floating PV and building-integrated PV (BIPV), unique thermal characteristics introduce additional complexities. Floating PV systems benefit from the cooling effect of water, yet seasonal variations in water temperature significantly influence convective heat transfer, requiring modified thermal coefficients for accuracy [55]. Similarly, BIPV systems experience distinct thermal behaviors due to ventilation gaps, façade design, and the thermal mass of buildings, with recent studies demonstrating considerable variation in thermal coefficients depending on the integration strategy [56]. These challenges underscore the need for further research in developing robust, adaptable thermal models that integrate both empirical and data-driven approaches to improve the accuracy of temperature predictions across diverse PV system designs.

The PV operation in Short circuit (SC) and open circuit (OC) status are some of the most serious faults that need to be detected and avoided [57]. A short circuit can be caused by many reasons some of which are poor wiring, damaged junction box, animal damage, water infiltration, and faulty bypass diode. It can happen between two points in the same string or between different strings [58]. Open circuit (OC), on the other hand, occurs when module terminals are disconnected, making the current of all the modules in the same string zero. Such faults are often caused by broken cells, damaged connections between them, loose connections, and defected power cables due to aging [59]. An integrated maximum power point (MPP) tracking algorithm allows the extraction of the maximum power possible from the PV module [60]. The voltage and the current of the MPP are around 80 % and 90 % of the open circuit and short circuit, respectively, depending on the module specifications [61]. When a PV system operates in a point other than the MPP, part of the electrical energy that wasn't absorbed by the module is converted to another form of energy, mostly thermal energy, elevating the module temperature [62]. While most studies have focused on MPP operation as the primary goal for maximizing energy production, less attention has been given to evaluating performance at operating points other than the MPP condition. Kurnik et al. [63] performed an experimental and prediction evaluation of PV module installed in different mounting configuration; open rack and isolated rooftop operating in both open circuit and maximum power point conditions. The thermal modeling was based on a linear relationship but has been enhanced with a

nonlinear approach using the energy balance model while representing the open circuit condition as a no electrical efficacy in the thermal modeling. The effect of different electrical operating conditions on PV thermal performance is shown to be significant and dependent on the module's actual conversion efficiency. Ciulla et al. [64] developed an implicit correlation that considers standard weather variables and the electrical production regimes of PV modules, demonstrating great potential. However, the developed thermal models include coefficients that must be empirically determined for each PV module. Moreover, there is no explanation regarding the testing of the developed model under different electrical production regimes.

As solar costs continue to decline, societal pressures for increased renewable energy adoption are growing. This trend is driving the transition from a conventional power system dominated by dispatchable generation to one where PV becomes the primary energy source [65]. Consequently, the focus of solar resource management must shift from balancing short-term fluctuations to ensuring reliable power supply 24/365, even during periods of low or null solar irradiation. To achieve this, a combination of strategies is necessary, including energy storage, demand-side flexibility, and geographic diversification of PV installations. Additionally, overbuilding PV capacity and proactively curtailing excess generation during periods of high solar output are emerging as a viable solution to address the inherent intermittency of solar power [66].

Traditionally, grid management has operated on matching power generation with immediate consumption or storage. As a result, over-building PV capacity and intentionally curtailing excess generation has been considered inefficient and wasteful. However, recent studies have challenged this conventional wisdom [66–68]. By strategically over-building PV systems and selectively curtailing output during periods of high solar irradiation, it is possible to significantly reduce the cost of providing firm, dispatchable solar power. This approach leverages the inherent variability of solar energy to achieve a more reliable and cost-effective power system.

**As a matter of fact, the possibility that the grid-connected photovoltaic systems will work in operating points different from the maximum power point will be more and more probable.** During the real operating condition, the PV module can operate at a voltage higher than one of the MPP or at a current higher than one of the MPP, causing a significant reduction in the module productivity. It is reported that such faults can stimulate thermal stresses, especially short circuit faults, which could lead to fire hazards in some conditions [69]. For example, for the off-grid systems [70–72], the Pulse-width modulation (PWM) charge controller operates at a lower operating area than the MPP point, after the state of charge of the battery, diverting the PV system's production closer to the short circuit current value of the module [73], making the PV module more likely to be from a hotspot [74]. With the development of new installation solutions and technologies, it was necessary to have a reliable standard operating procedure, which was provided by international initiatives such as the International Energy Agency (IEA) and the Photovoltaic Power Systems Program (PVPS) Task 13 [58].

Based on the aforementioned literature, it can be concluded that most of the thermal studies conducted on PV systems were focused on the effect of meteorological variables on the thermal performance of solar cells, as well as an attempt to improve and reduce the module temperature and quantify the corresponding improvement in the electrical performance. Several thermal models were developed for older, low-efficiency PV modules and have not been updated to reflect advancements in modern module technologies. This lack of updates leads to inaccuracies in temperature estimation, potentially affecting performance evaluation.

Moreover, the impact of the electrical operating status on the thermal performance of PV modules is often overlooked. To the best of our knowledge, no **existing literature investigates the thermal behavior of PV modules under Maximum Power Point (MPP), Open-Circuit (OC),**

and Short-Circuit (SC) conditions simultaneously. While previous research examines the OC condition, it does not provide insights into the thermal behavior under SC conditions, which can perform significantly differ. Even thermal models that incorporate real-time voltage measurements are primarily developed for module operation at the MPP, leaving scenarios outside this maximum power point unexplored. Furthermore, thermal models typically fail to adequately address the influence of the electrical operating status of PV modules on their thermal behavior. The emerging necessity for photovoltaic (PV) systems to operate at points other than the Maximum Power Point (MPP)—due to factors such as overgeneration (e.g., curtailment) or the need to provide primary frequency reserves—underscores the importance of examining the accuracy of current thermal models under different electrical operating conditions.

Accordingly, the thermal behavior of the PV module responding to different extremes of real electrical operating statuses, including the open circuit (OC), short circuit (SC), and maximum power point (MPP) operating, is considered in the present study. To achieve these goals, three sets of rooftop monofacial PV systems, each operating at the aforementioned electrical operating status, are utilized to have simultaneous performance evaluation under the same meteorological conditions. Thermal images of the PV sets operating at different electrical statuses are used to provide in-detail scanning for hotspots or any abnormality that shall affect the temperature distribution of the module itself at these electrical operating statuses.

For better insight into thermal modeling, a comprehensive comparison has been conducted with the most widely used thermal models in the literature and those recommended by standards. This comparison evaluates their accuracy for systems operating under different electrical conditions. The examined models are static models frequently cited in the literature and commonly used in commercial simulation software, along with their widely referenced coefficients, which can be applied for online monitoring. The adopted thermal models have been classified according to the number of meteorological variables. A radiation-sensitive analysis has been conducted to estimate these thermal models compared to the measured temperature, considering the three different electrical operating statuses. The objective of the present work has been executed as follows: 1. Introduction includes a survey about the thermal performance of the PV module that may include the influence of the electrical operating status; 2. The in detail explanations of the built experimental setup and the methodology adopted; 3. An energetic balance to the three electrical operating statuses and stating the thermal models considered; 4. Results and its discussion include the different thermal performance between the three named electrical statuses and a sensitive comparison between the examined thermal models; and finally 5. Conclusion of the proposed investigation with a recommendation for upcoming studies.

## 2. Experimental test setup and measurement devices

### 2.1. Experimental setup

The experimental setup was built on the rooftop of the Faculty of Engineering building at Jaén University campus in Spain. The experimental setup consists of three sets of PV systems, each operating in different extreme electrical statutes: short-circuited (PV set-1), open-circuited (PV set-2), and operating at maximum power point (MPP) (PV set-3). Each set consists of two identical monofacial PV modules connected in parallel. The characteristics of the 6 typical PV modules can be seen in Table 1. A free-standing rooftop mounting has been adopted in installing the three PV sets oriented to the south, as can be seen in Fig. 1. The PV rack is fixed 1.5 m high from the roof surface.

### 2.2. Instrumentations & DAQ system

The meteorological parameters presented in the plane of array

**Table 1**  
Specification of the PV module.

| Specification  | Value           |
|--|-----------------|
| Model name   | WS-100/12V      |
| Panel brand  | WAAREE          |
| Material   | Polycrystalline |
| Dimensions in mm   | 1150 × 675 × 35 |
| Short-circuit current ( $I_{sc}$ ) [A]                                       | 6.07            |
| Open circuit voltage ( $V_{oc}$ ) [V]  | 21.97           |
| Maximum power ( $P_{MP}$ ) [W]   | 100             |
| Maximum power voltage ( $V_{MP}$ ) [V]                                       | 17.47           |
| Maximum power current ( $I_{MP}$ ) [A]                                       | 5.73            |
| Open circuit voltage temperature coefficient [ $^{\circ}/^{\circ}\text{C}$ ] | -0.2941         |
| Maximum power temperature coefficient [ $^{\circ}/^{\circ}\text{C}$ ]        | -0.3845         |
| Nominal Operating Cell Temperature [ $^{\circ}\text{C}$ ]                    | 46              |
| Module efficiency at standard test conditions, ( $\eta_{STC}$ ) [%]          | 12.88           |

radiation ( $G_{POA}$ ), wind speed ( $\omega$ ), and ambient temperature ( $T_a$ ) are the main driving recorded variables affecting both thermal and electrical operating conditions of the PV systems. The plane of array irradiance was measured by DATASOL MET installed above the module parallel to the PV modules' plane, see Fig. 1. DATASOL MET is a calibrated reference cell used to sense the intensity of the received radiation at the installed plane. Moreover, an anemometer is used to measure the ambient wind speed that directly impacts the installed PV modules. The ambient temperature was gauged by an ambient temperature thermometer installed 5 m away from the experimental setup to avoid thermal interaction with the PV modules.

The thermal performance of the three sets of examined PV modules was assessed using temperature sensors and thermal imaging. A high-precision PT100 temperature sensor was installed on the rear surface of one of the two PV modules in each set. Additionally, a surface-type PT100 sensor was placed at the centre of the back of each module, following IEC 61724-1 standard guidelines [75]. A periodic check of PV module temperatures was conducted to ensure measurement consistency. The three PT100 sensors were directly connected to the NI data acquisition system, as shown in the schematic diagram of the experimental methodology (Fig. 2). The estimated uncertainty in the temperature measurements, including the temperature sensor and the data acquisition, is 0.81 °C, which confirms the reliability of the monitoring system adopted. Furthermore, a Fluke TiS20+ thermal imaging camera was used to capture the temperature distribution across the PV module surface. Thermal images were taken for three different sets—short-circuited, open-circuited, and MPP-operating modules—to provide deeper insight into the impact of electrical operating conditions on thermal behavior. Outdoor thermography images were captured with a minimum solar irradiance of 600 W/m<sup>2</sup> to clearly identify temperature distribution and detect any potential failures [76]. Thermal images of both the front and back of the PV modules were taken periodically every 30 min during the noon periods of sunny days.

Infrared (IR) images were compared with thermocouple data to verify the accuracy of the single-point measurements. This comparison also ensured that thermocouple readings were not influenced by localized hot spots, thereby improving measurement reliability. It is worth noting that temperature distribution across the module can be affected by non-uniform irradiance, wind speed variations (e.g., turbulence), and PV cell electrical mismatch. Since these factors are time-dependent and dynamic, accurately characterizing their impact remains challenging.

The electrical performance of short-circuited PV set-1 ( $V = 0$ ,  $I = I_{sc}$ ) and open-circuited PV set-2 ( $V=V_{oc}$ ,  $I = 0$ ) has been monitored by the data acquisition devices. Such monitoring guarantees the operation at specific fixed points. However, PV set-3 has been designed to operate at the maximum power point (MPP). Electronic load EL9000B is used to track the MPP of PV set-3 at different ambient conditions. The electronic load EL9000B features a maximum power point tracking (MPPT) algorithm that tracks the global MPP, which is software-controlled. The reading of the maximum power voltage and current is used directly for



**Fig. 1.** Photograph of the experimental apparatus at the University of Jaén (Spain).

real-time monitoring and analysis applications developed on LabVIEW software, see Fig. 2.

Table 2 shows the features of the monitoring devices along with their accuracy; (a). The expression introduced in Ref. [77] is utilized to express the standard uncertainty for a per instrument,  $u$ :

$$u = \frac{a}{\sqrt{3}} \quad (1)$$

### 3. Energetic analysis

Thermal modeling of the PV module mostly depended on the thermal balance between the incoming radiation, generated electric energy, and the thermal losses from the module, as can be expressed in the following expression [78]:

$$E_{in} = E_{out} + \varphi_{gen} + \frac{dE_{syst}}{dt} \quad (2)$$

Where:

$E_{in}$ : The energy entering the PV system, which is mainly the captured plane of array radiation ( $E_{POA}$ ).

$\varphi_{gen}$ : The thermal energy generated in the system, which usually is made by joule losses resulting from an electric current flow through the PV cells in the module and the transformation of a partition of the solar spectrum into heat.

$E_{out}$ : The energy exiting the PV system, which is made of the output electrical energy ( $E_{PV}$ ) and heat exchange between the PV module and the environment by radiation  $Q_{rad}$  and convection  $Q_{conv}$

$\frac{dE_{syst}}{dt}$ : This term represents the rate of changing internal energy of the PV module (the module temperature).

While the incoming radiation is mainly dependent on the environmental condition, among other parameters, the heat generation and the electrical power out from the module depend on the load connected to the module, defining the electrical operating point in the I-V characteristic curve. Focusing on the possible electrical operating status of a PV module reveals that its thermal behavior can be influenced by the electrical status. These conditions can be categorized into three regimes, each with extreme operating points.

- The first regime is identified by a low power production and high current (including the short circuit current as an extreme operating point) and relatively low voltage value ( $V/V_{MP} < 0.95$ ) where the I-V characteristic can be considered almost parallel to the x-axis, Fig. 3-a. For a very low voltage, the current flow within the module between its terminals faces a low resistance except for the internal resistance of the solar cells themselves and interconnections. This leads to electrical power dissipation in the form of heat, a phenomenon known as Joule heating, representing internal heat generation. The power dissipated as heat is proportional to the square of the current. This generated heat causes the temperature of the PV module to rise. Since the short-circuit operation allows for the highest current, the Joule heating effect is at its maximum, leading to a higher module temperature.
- The second regime is characterized by maximum power point on the IV curve. When a PV module is operating in this area, it's driven by an MPP algorithm extracting the maximum power possible. It can be defined with a voltage ratio limitation of  $0.95 < V/V_{MP} < 1.05$ , see Fig. 3-b In this regime, the transformation is maximized, with the incoming radiation being converted into electrical power and heat transfer via convection and radiation, all the incoming radiation is

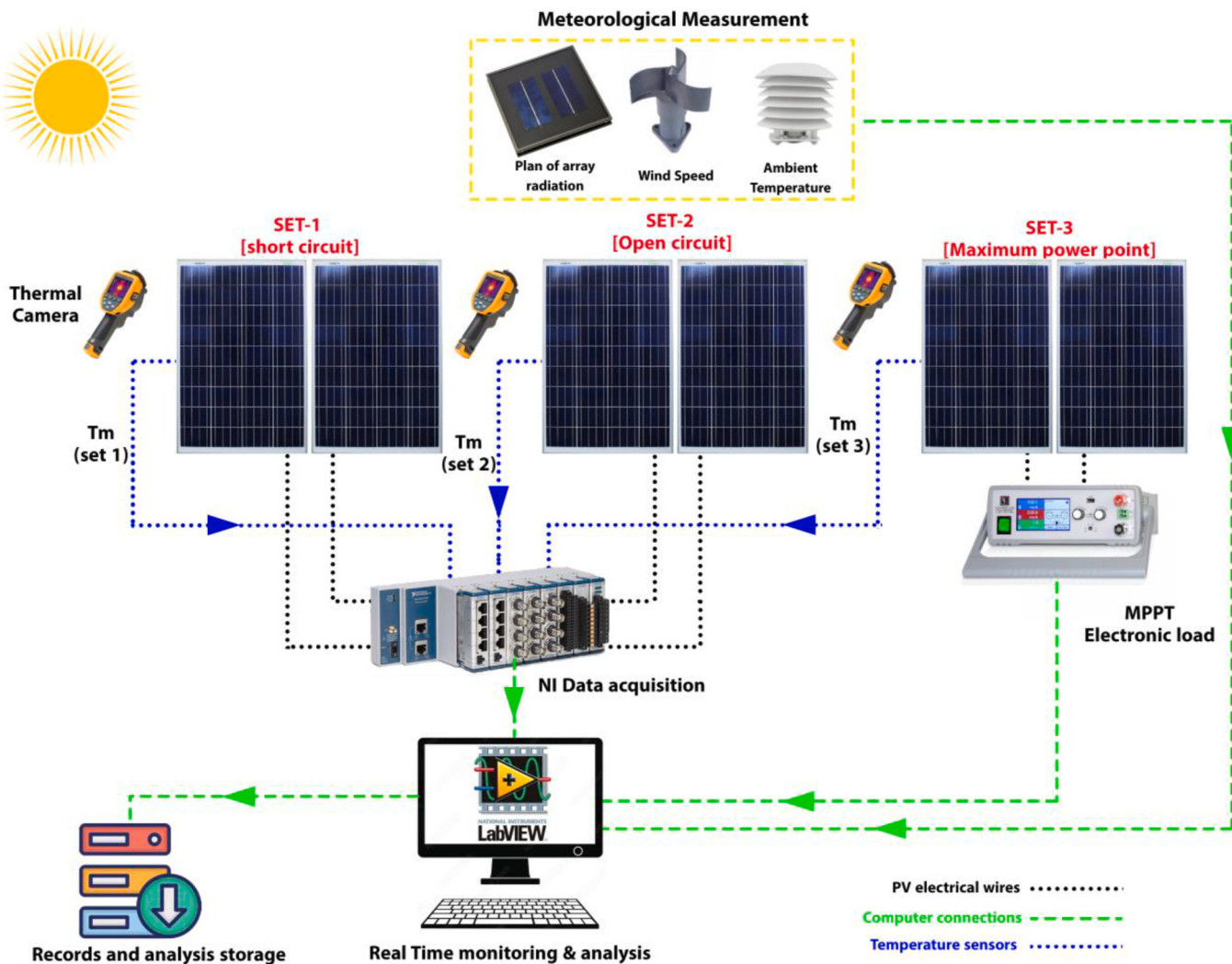


Fig. 2. Schematic diagram of the experimental setup.

**Table 2**  
Accuracy and uncertainty of devices.

| Devices                  | Measured parameter           | Brand        | Accuracy                 | Standard uncertainty |
|--------------------------|------------------------------|--------------|--------------------------|----------------------|
| PT100 temperature sensor | PV module temperature        | –            | 0.15 °C                  | 0.086 °C             |
| Thermal camera           | Temperature distribution map | Fluke TiS20+ | ±2 % or ±2 °C            | 1.15 %               |
| Calibrated PV cell       | Plane of array radiation     | DATASOL MET  | ±2.2 %                   | 1.27 %               |
| Anemometer               | Wind speed                   | DATASOL MET  | 0.27 m/s (0.83–4.16 m/s) | 0.15 m/s             |

converted to the electrical power and heat transfer via convection and radiation achieving the balance with the internal energy (module temperature).

- The third regime is characterized by a high voltage value (including the open circuit voltage as an extreme operating point). In this regime, when the ratio  $V/V_{MP} > 1.05$ , the power production is deteriorated by sharp linear decrement of the current reaching the open circuit point where there is no power is produced  $P = 0$  ( $I = 0$ ,  $V = V_{oc}$ ), as can be noticed in Fig. 3-c. In open circuit operation at  $V_{oc}$ ,

no current flows, and there is minimal Joule heating within the PV cells. The heat accumulated in the module is due to the absorption of sunlight, which primarily warms the surface and cells due to solar irradiance but does not significantly increase temperature through electrical losses.

### 3.1. Thermal models

Several simplified thermal models have been developed to determine the PV cell temperature ( $T_c$ )—the temperature of the solar cells inside the module—while others focus on calculating the module temperature ( $T_m$ ), which is the back surface temperature of the PV module. These models typically adopt steady-state thermal analysis to estimate temperatures under various operating conditions. Many models are based on the energy balance for steady-state conditions, in which the thermal capacity of the PV module and transient response are neglected, and others are developed based on empirical datasets as multivariate regression models [79]. The variables considered in the models usually are plane of array irradiance ( $G_{POA}$ ), ambient temperature ( $T_a$ ), and, in some cases, wind speed ( $\omega$ ) [24]. PV simulation software tools utilize thermal models to quantify the impact of the temperature of PV cells on the expected generated power, frequently reported as 1-h averages or less, depending on the tool applied. In this paper, four models are considered. Specifically, models have been selected because they are

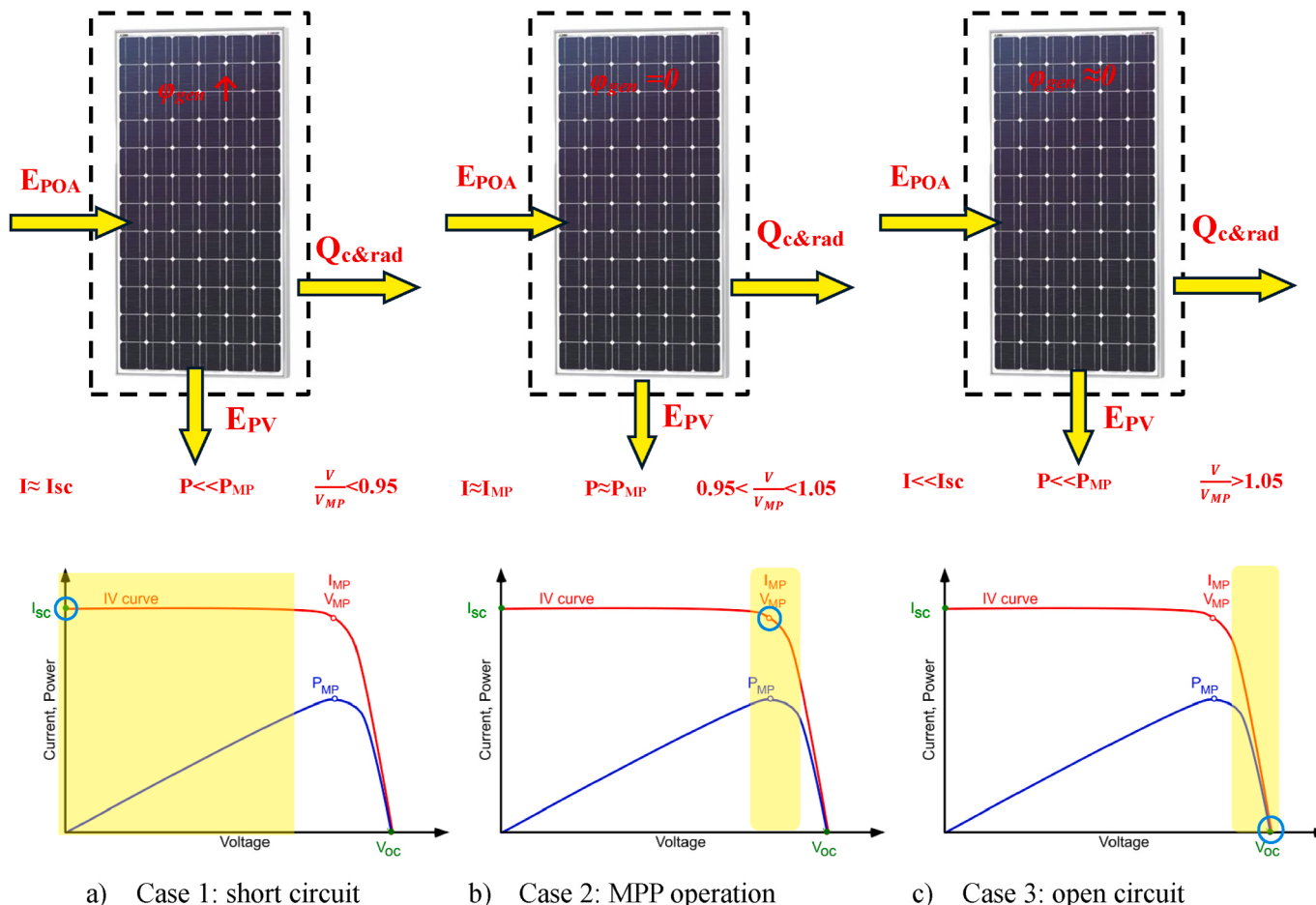


Fig. 3. Graphical representation of an energy balance of three regimes of the IV curve.

either used in major photovoltaic software tools, cited in IEC standards or report the efficiency of the PV module. In the following paragraph, they are presented and discussed, and they are classified according to the number of variables.

### 3.2. Two variable-based thermal model

- Nominal Operating Cell Temperature (NOCT) model

Standard Model, also known as Nominal Operating Cell Temperature (NOCT) model [80], is the most common model to estimate the cell temperature of a PV module [81]. NOCT model is a simplified steady-state model where the cell temperature,  $T_c$ , is expressed as a function of the plane of array irradiance,  $G_{POA}$ , and the ambient temperature,  $T_a$ . The expression

$$T_c = T_a + G_{POA} \cdot \left( \frac{T_{c,NOCT} - T_{a,NOCT}}{G_{POA,NOCT}} \right) \quad (3)$$

Where:

$T_{c,NOCT}$  is a temperature parameter provided by the manufacturer of the PV module in the datasheet. It is measured according to the standard IEC 61215–2:2016 [82] under the operating conditions:  $T_{a,NOCT} = 20^\circ\text{C}$ ,  $G_{POA, NOCT} = 800\text{W/m}^2$ ,  $\omega = 1\text{ m/s}$ . Further NOCT value is measured with a PV module in an open circuit, yet it doesn't include any information about the mounting configuration [83].

### 3.3. Three variable-based thermal models

Faiman model, Sandia model, and Duffie and Beckman model are

some of the most famous models adopted by several commercial PV software tools and recommended by the standard IEC TS 61724 [84]. Moreover, among the continuous efforts that focus on improving thermal modeling, Keddouda et al. [85] recently developed a modification based on mathematical formula of Sanida model. These models have three meteorological variables: plane of array irradiance, ambient temperature, and wind speed.

- Faiman model:

Faiman model [86] was developed based on the hypothesis of considering the PV module is a flat-plate solar-thermal collector under conditions of steady-state using Hottel–Whillier–Bliss equation [87]. The electrical efficiency of the module was considered from an energy balance point of view. The model was built based on the experimental examination of mc-Si and pc-Si cells with front glass covers and Tedlar back operating in maximum power conditions at Sede Boqer in the Negev Desert - East Sinai Peninsula. The Faiman model can be expressed as follows:

$$T_c = T_a + \frac{\alpha G_{POA} (1 - \eta_e)}{U_c + U_v \omega} \quad (4)$$

Where:

$U_c$ : Coefficient describing the effect of the radiation on the module temperature [ $\text{W/m}^2\text{C}$ ].

$U_v$ : Coefficient describing the cooling by the wind [ $\text{W.s/m}^3\text{C}$ ].

$\alpha$ : Module absorption coefficient  $\approx 0.9$  [88].

$\eta_e$ : the electrical efficiency of the module at maximum power point As  $U_c$  and  $U_v$  coefficients are very sensitive to the installation

configuration, several studies [22,38] specified these coefficients for selected technologies of PV modules, which can be selected for rooftop monofacial PV modules to be ( $U_c = 25 \text{ W/m}^2\text{C}$ ,  $U_v = 1.2 \text{ W s/m}^3\text{.}^\circ\text{C}$ ).

### • Exponential thermal models

There are some thermal models where the dependency on wind speed is expressed by an exponential function; in Eq. (5), the general expression is reported in two possible forms:

$$T_m = c_1 \cdot T_a + c_2 \cdot G_{POA} \cdot e^{c_3 \cdot \omega} = c_1 \cdot T_a + G_{POA} \cdot e^{c_4 + c_3 \cdot \omega} \quad (5)$$

Where  $T_m$  is the module temperature, the following sections present the Sandia and Keddouda models, as described in equation (5).

### • Sandia model

Sandia model [26] is a simplified empirical thermal model developed in Sandia National Laboratories. It is worth mentioning that the thermal model was developed based on an energy balance considering the thermal mass of the PV module and better consideration for the thermal analysis, yet no mention of the electrical connection condition of the PV module, whether it's electrically loaded or not [89]. The module temperature of the PV module estimated by this model depends on the main meteorological parameter, as can be seen in the following equation [90]:

$$T_m = T_a + G_{POA} \cdot e^{a+b \cdot \omega_{10}} \quad (6)$$

$$\omega_{10} = \omega \cdot \left( \frac{H_{10}}{H} \right)^{\xi} \quad (7)$$

Where:

$T_m$ : The module temperature, [ $^\circ\text{C}$ ].

$\omega_{10}$ : The wind speed corrected to 10m height or to the height that is relevant to the power model [m/s].

$\omega$ : The measured wind speed (2 m above the ground or 0.5 m above the module) [m/s].

$H_{10}$ : The height used by the performance model (typically 10m) [m].

$H$ : The above grade anemometer height [m].

$\xi$ : The resistance coefficient for ground cover or the Hellmann exponent

a: Empirically determined coefficient establishing the upper limit for module temperature

b: Empirically determined coefficient establishing the rate at which module temperature drops as the wind speed increases.

For an open rack-mounted monofacial PV module (Glass/cell/polymer sheet), the coefficients a and b are  $-3.56$  and  $-0.075$ , respectively. Sandia model can provide the anticipated  $T_m$  with an accuracy of around  $5 \text{ }^\circ\text{C}$ , which proves the flexibility and appropriateness for system engineering and design objectives [23].

While the Sandia model directly calculates the module temperature ( $T_m$ ), the PV cell temperature ( $T_c$ ) is the temperature of the solar cells inside the module, which can be determined using a simple heat balance equation. This equation accounts for the conductive temperature drop across the PV module and is expressed as follows: [49], given the  $T_m$ :

$$T_c = T_m + \Delta T \cdot \frac{G_{POA}}{1000} \quad (8)$$

Where  $\Delta T$  is the temperature difference between the cell and module back surface in the level of irradiance of  $1000 \text{ W/m}^2$ . Its value is very sensitive to the type of module and the mounting. For the open rack installation of the Glass/cell/Polymer sheet module,  $\Delta T = 3 \text{ }^\circ\text{C}$ .

Recently, Keddouda et al. [85] performed a modification on the thermal model that follows the exponential mathematical formula as the Sandia model. The thermal models developed based on comprehensive three-dimensional CFD simulation of poly-Si photovoltaic modules, as

can be seen in Eq. (9). It was reported that the developed models have more accuracy compared to Ross [91], King [26], and Skoplaki [92] models. The experimental validation conducted at El Oued University, Algeria, over a three-day period, confirms the accuracy of the developed coefficients. The wind speed used in Eq. (9) was measured at a height of 2 m above the ground or 0.5 m above the module, ensuring consistency with the modeling assumptions.

$$T_m = 0.905T_a + 0.0291G_{POA}e^{-0.031\omega} \quad (9)$$

### • Duffie and Beckman model

In this approach, thermal modeling is based on an energy balance between the parameters affecting the changing of the module temperatures. The solar energy absorbed by a module is converted to thermal and electrical energy, which is removed from the cell through the external circuit. An energy balance on a unit area of a module while considering the thermal losses by convection, conduction, and radiation. It is worth mentioning that such a thermal model is adopted via the SAM simulation software tool. The cell temperature of the PV module can be expressed as the following [20,93]:

$$T_c = T_a + \left( \frac{9.5}{5.7 + 3.8 \cdot \omega} \right) \frac{G_{POA}}{G_{POA,NOCT}} (T_{c,NOCT} - T_{a,NOCT}) \left( 1 - \frac{\eta_e}{\tau a} \right) \quad (10)$$

Where  $\omega$  is the measured wind speed (2 m above the ground or 0.5 m above the module), [m/s] and  $\tau a$ : product of transmissivity and absorbanace coefficients  $\approx 0.9$  [94].

According to the literature, it can be reported that all stated thermal models have been developed and tested under the assumption that the PV modules operate at the maximum power point in the models where the electrical efficiency is considered (Faiman and Duffie&Beckman); it is considered constant and calculated under standard test conditions (STC). This means that such models have to be specifically tested to verify their precision under different electrical operating conditions. The extension of Faiman and Duffie&Beckman models at short circuit and open circuit conditions is obtained, imposing an electrical efficiency equal to zero ( $\eta_e = 0$ ). In the next paragraphs, the precision of the considered models (with and without the assumption about the electrical efficiency) is verified experimentally. A summary of the examined thermal models in the present studies is presented in Table 3

### 3.4. Statistical evaluation

To evaluate the precision of the mentioned models against the experimental measurements with different electrical operating points in real-use conditions, statistical metrics are introduced [95]. The Mean absolute error (MAE), Root Mean Square error (RMSE), and Mean Absolute Percentage Error (MAPE) are utilized for error estimation, as can

Table 3

Summary of examined thermal models in the current study.

| Thermal model            | Ref. | Eq. No.  | Equation  | coefficients                        |
|--------------------------|------|----------|---|-------------------------------------|
| NOCT model               | [80] | Eq. (3)  | $T_c = T_a + G_{POA} \cdot \left( \frac{T_{c,NOCT} - T_{a,NOCT}}{G_{POA,NOCT}} \right)$   | -                                   |
| Faiman model             | [27] | Eq. (4)  | $T_c = T_a + \frac{aG_{POA}(1 - \eta_e)}{U_c + U_v \cdot \omega}$   | $U_c = 25 \text{ W/m}^2$<br>$= 1.2$ |
| Sandia model             | [26] | Eq. (6)  | $T_m = T_a + G_{POA} e^{a+b \cdot \omega_{10}}$   | $a = -3.56$<br>$b = -0.075$         |
| Keddouda model           | [85] | Eq. (9)  | $T_m = 0.905T_a + 0.0291G_{POA}e^{-0.031\omega}$  | -                                   |
| Duffie and Beckman model | [20] | Eq. (10) | $T_c = T_a + \left( \frac{9.5}{5.7 + 3.8 \cdot \omega} \right) \frac{G_{POA}}{G_{POA,NOCT}} (T_{c,NOCT} - T_{a,NOCT}) \left( 1 - \frac{\eta_e}{\tau a} \right)$ | -                                   |

be expressed in the following formula [96,97].

$$MAE = \frac{1}{n} \sum_{i=1}^n |y_{i,m} - y_{i,c}| \quad (11)$$

$$MAPE = \frac{1}{n} \sum_{i=1}^n \left| \frac{y_{i,m} - y_{i,c}}{y_{i,m}} \right| \quad (12)$$

$$RMSE = \sqrt{\frac{1}{n} \sum_{i=1}^n (y_{i,m} - y_{i,c})^2} \quad (13)$$

where  $y_{i,m}$  and  $y_{i,c}$  are the measured and calculated temperatures, respectively. On the other hand, n is the number of samples.

#### 4. Results and discussion

The monitoring of the thermal and electrical performance took place over four months, from March to June 2024. The recording interval is 30 s, which has been averaged on a 5-min basis. For system reliability before starting the analysis, the three PV sets were operating in an open circuit to confirm the consistency between the sensor readings installed in the three sets. The electrical and thermal measurement, including temperature sensor readings and thermal images, confirms the reliability and consistency of the three PV sets. It is also worth mentioning that measurements of the short-circuited PV set 1 took place on some selected days to avoid permanent faults that could affect the health of the modules.

##### 4.1. Thermal assessment of PV systems with different electrical operating statuses

During four months-monitoring of the thermal performance presenting in the module temperature of the PV sets operating at OC, SC, and MPP operation is summarized in Fig. 4, presenting the daily

monthly module temperature with the corresponding irradiance. It can be seen that the short-circuited PV set 1 has the highest module temperature ( $T_{m-SC}$ ) compared to the other two situations (open-circuited PV set 2 module temperature ( $T_{m-OC}$ ) and temperature of PV set-3 module operates in MPP ( $T_{m-MPP}$ )). Depending on the received irradiance and ambient condition, the temperature of the short-circuited PV module is 4.30 °C–9.35 °C higher than the module operates in MPP. In comparison, the temperature of the open-circuited PV module is 2.16 °C–4.35 °C higher than the MPP operating one, as can be seen in Fig. 4.

To explore the thermal performance at different electrical operating statuses, a sample of the measurements taken during the monitoring period is examined closely. A clear sky day in a continental climate location has been considered to examine the thermal response of such phenomena. Records captured during the 18th of May representing the meteorological variables and the corresponding thermal response of the PV sets operating at OC, SC, and MPP operation presented in Fig. 5. The measured meteorological variables show that the elevated plane of array irradiance reaching the maximum value of 917 W/m<sup>2</sup> with an average ambient temperature of 18.90 °C and wind speed around 1 m/s during that day. In Fig. 5, it can be noticed that PV set-3 operating at MPP has a comparatively lower module temperature, especially at a high level of radiation. The daily average of the  $T_{m-SC}$  is 46.63 °C, while for the  $T_{m-OC}$  is 42.91 °C. However, PV set-3 operating at MPP has an average module temperature of  $T_{m-MPP} = 39.71$  °C. This means that on a daily basis, considering only solar hours, when the PV module operates at MPP, the mean module temperature is 17.41 % less than a short-circuited PV module and 8.01 % less than the open-circuited module. It can also be observed that, regardless of the electrical operating state, the module temperature at night is consistently lower than the ambient temperature by approximately 2–4 °C. This phenomenon can be attributed to radiative cooling during cloudless nights. In the absence of incoming solar radiation to counterbalance the thermal radiation emitted by the PV modules toward the cold sky, the module temperature drops below the ambient temperature. This highlights the interaction between PV modules and their thermal environment, underscoring the importance of

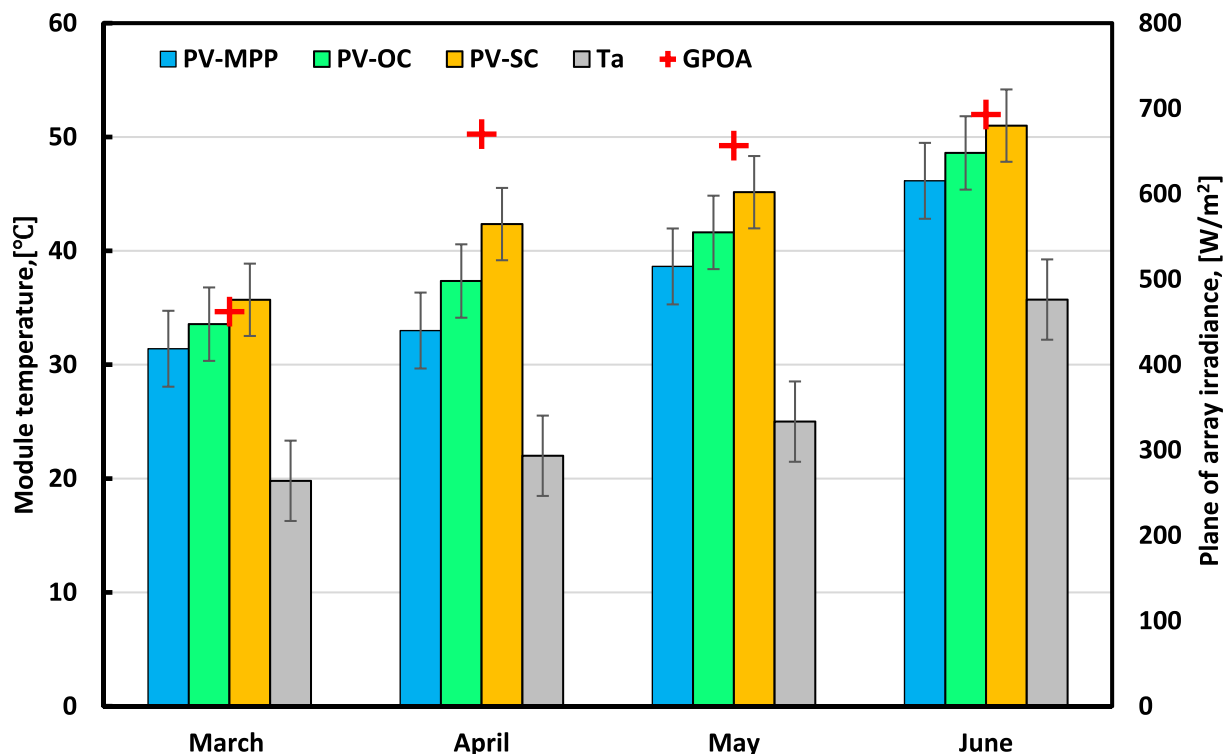


**Fig. 4.** Monthly average of daily irradiance (GPOA) and the measured PV module temperature that operates in short circuit (SC), open circuit (OC), and maximum power point (MPP) conditions including the standard error of the temperature measurements in each bar.

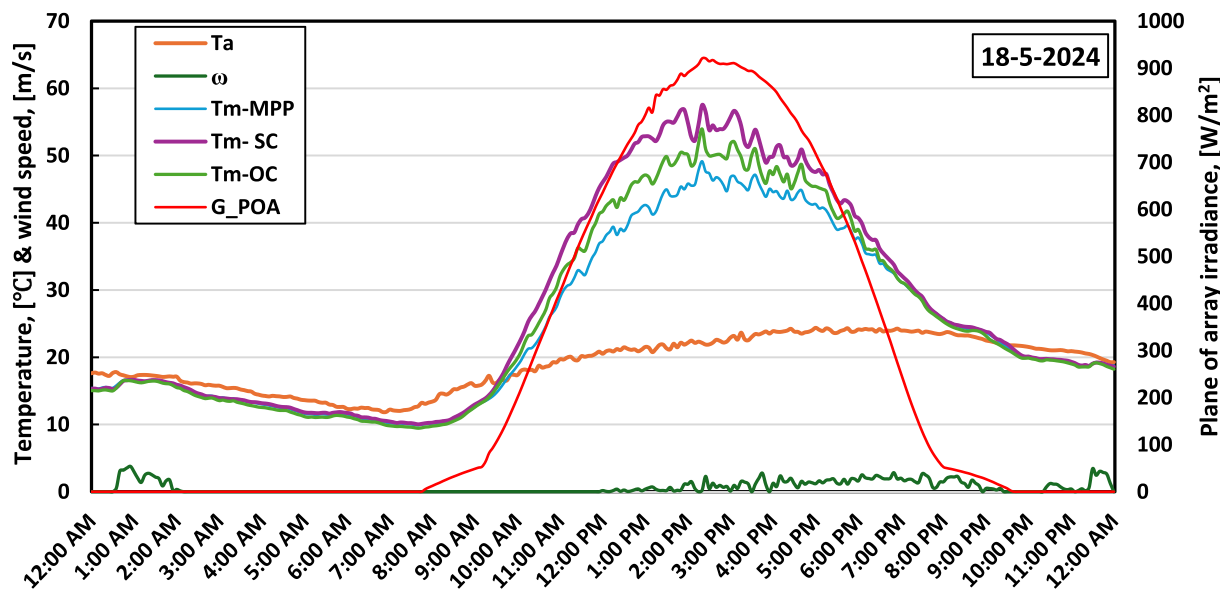


**Fig. 5.** Example of daily measured variables (5 min) time step: ambient variables (ambient temperature, wind speed and POA irradiance) and PV module temperatures at SC, OC and MPP operating conditions.

accounting for nocturnal radiative heat exchange in thermal modeling and energy yield assessments.

By taking a closer look at the thermal response of the PV modules operating in different electrical statuses with respect to various intensities of received irradiance, see Fig. 6. It can be noticed that for levels of radiation lower than  $200 \text{ W/m}^2$ , the PV module temperatures with different electrical operation statuses have a similar value with an insignificant variation. Moreover, for levels of radiation higher than  $200 \text{ W/m}^2$ , a liner increment in the module temperature with different slopes with respect to the electrical operating status of the PV module, especially during the heating up of the module. At a high level of irradiance reaching  $900 \text{ W/m}^2$ , the temperature difference between the sets, relative to the MPP operating PV set, can reach  $10^\circ\text{C}$ . While during the

cooling down (the reduction of the solar irradiance intensity from the solar noon to the sunset), the temperatures of both short-circuited module and open-circuited module exhibit more similar values than the PV module operates at MPP achieve a lower temperature for the same level of radiation.

Such temperature variation between the PV sets with different electrical operating statuses can be explained by an energy balance as in eq. (2). For the short-circuited PV set 1 and open-circuited PV set 2, no electrical energy is extracted from the system, meaning that all of the radiation energy is converted to a thermal one. Moreover, for PV set 1, the maximum value of current ( $I_{SC}$ ) flows through the PV module terminals, facing the resistance of the PV cells themselves, which in turn significantly increases the cell temperature. This can explain the

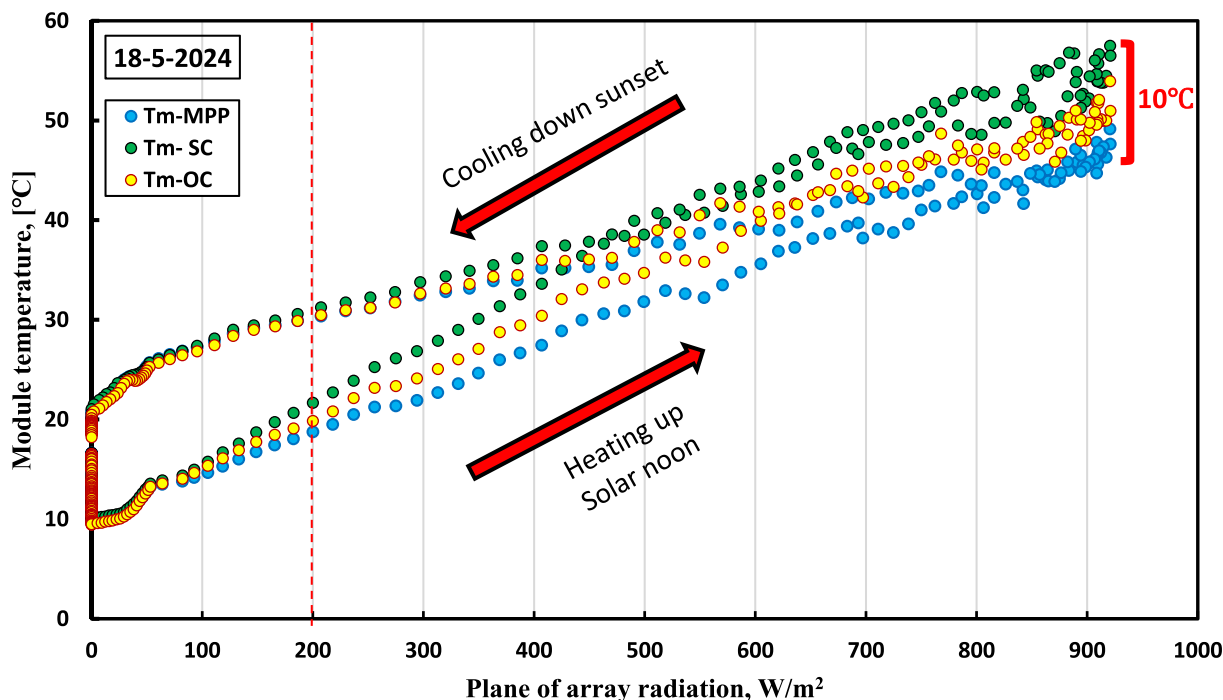


**Fig. 6.** Measured module temperature of PV sets against their corresponding radiation.

elevated module temperature of PV set-1 compared to open circuit ones in PV set-2. As for PV set-3, converting the received solar radiation with an electrical efficiency of around 12 % (depending on the module itself) and absorbing the maximum electrical power possible from the PV system significantly helps reduce thermal conversion.

While it's known that a module temperature represents the temperature of a point in the PV module, there is a nonuniformity temperature distribution across the active area of the module. Nevertheless, the hot spot is rarely captured by a temperature sensor. Thus, an infrared thermal image of the three sets is introduced in Fig. 7. It can be seen that there is a difference in the temperature between the three sets where PV set-3 has a more uniform yellowish color, presenting the lowest temperature between the sets. Moreover, the open-circuited PV set-3 has a uniform orange color along the modules' of the set, presenting a more elevated temperature. However, in the short-circuited PV set-1, a clear sign of hot spots (radish and white cells) is formed in both modules of the set. This thermal image is a clear sign of the hazard of short-circuited PV modules compared to the other electrical status examined.

#### 4.2. Thermal models assessment to various electrical operating statuses

The thermal models have been introduced to estimate the module temperature in case of the nonavailability of a temperature sensor and in the software tools for performance evaluation due to the vital rule of the module temperature in estimating the output power. Hence, the most common thermal models have been investigated against different electrical operating statuses considering short circuit, open circuit, and maximum power point. Some models, such as the NOCT model, Faiman model, and Duffie & Beckman model, estimate cell temperature ( $T_c$ ), while others, such as the Sandia model and Keddouda model, directly predict module temperature ( $T_m$ ).

For the thermal model assessments, temperature measurements were taken from the back surface of the PV module, providing the actual module temperature. To ensure a fair comparison, models that predict module temperature were directly compared with the measured values.

Meanwhile, thermal models estimating cell temperature were integrated with Eq. (8), which converts cell temperature to module temperature.

During the experimentation period, the module temperature was calculated for the corresponding meteorological condition considering the commonly used thermal coefficients in the literature, see Table 3, and compared with the relative measured module temperature for the three sets of PV systems operating at different electrical operating statuses. The calculated module temperature, using the aforementioned five thermal models to verify their behavior, for the sample day mentioned in Fig. 5 has been presented in Fig. 8.

It can be seen that the daily module temperature estimated by Duffie and Beckman was 44.45 °C, which suffers from the overestimation relative to the temperature of the MPP operating module. Moreover, it's so sensitive to the wind speed that it undergoes great fluctuation for wind gestures, as can be seen in Fig. 8. Simplifying Duffie&Beckman's model to a formula similar to Faiman models indicated that the wind speed coefficient ( $U_v = 11.61 [W/m^2°C]$ ) is significantly higher than the one considered in PVsyst ( $U_v = 1.2 [W/m^2°C]$ ). This can explain the high sensitivity to the wind speed, which in turn produced a highly fluctuated estimation that can be missed with its average precision. A high level of accuracy was found in the module temperature calculated by the Keddouda model during the day, as can be seen in Fig. 8 relative to the temperature of the MPP operating module, with a daily average value of 39.71 °C.

While calculated temperature via the Sandia model and Faiman model achieved a reasonable agreement with the module temperature operating at MPP, especially at high levels of radiation, the NOCT model tends to overestimate it. NOCT model was found to provide better precision to the measured open-circuited module temperature for high levels of radiation during the solar noon. It is noticed that at a low level of radiation, a minimum deviation in module temperature estimation using different models was found; nevertheless, it's electrical operating status.

For better evaluation of the thermal models' response to the different electrical operating statuses, a temperature difference between the

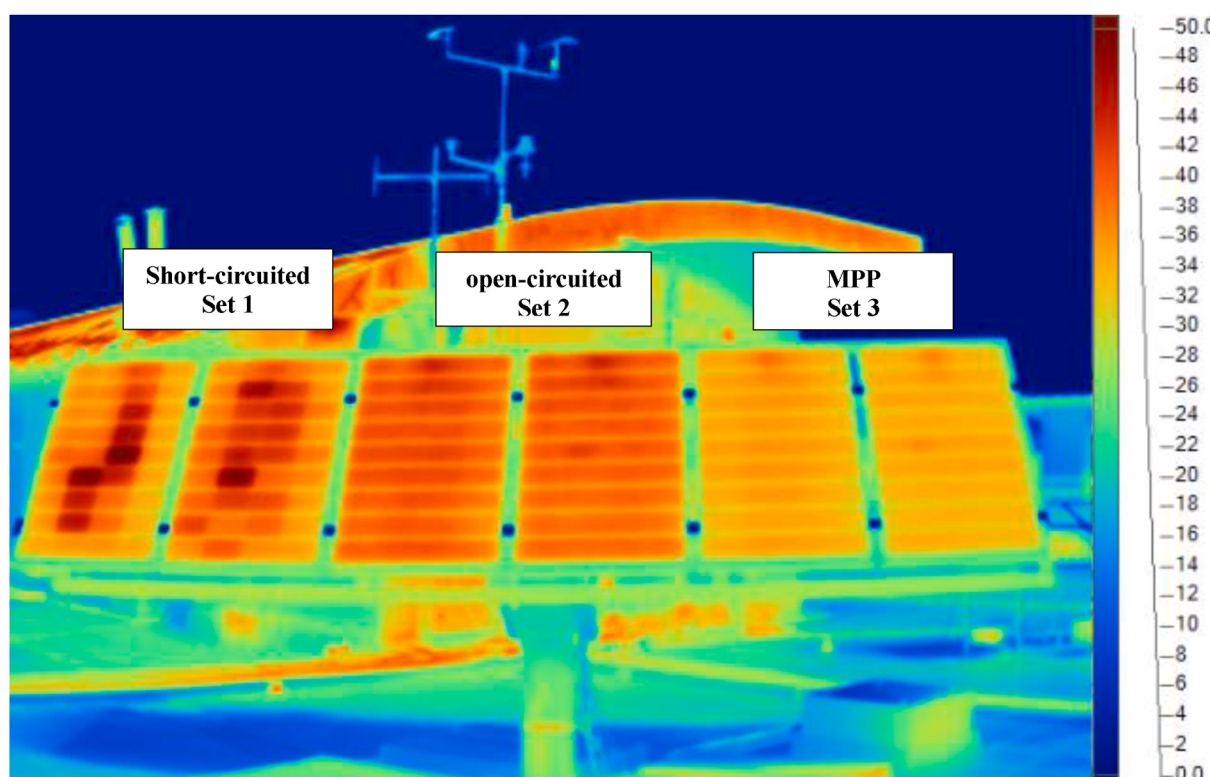


**Fig. 7.** Infrared thermal image of the three sets examining the three status of electrical connection ( $G_{POA} = 819 W/m^2$ ,  $T_a = 22.1 ^\circ C$ ).

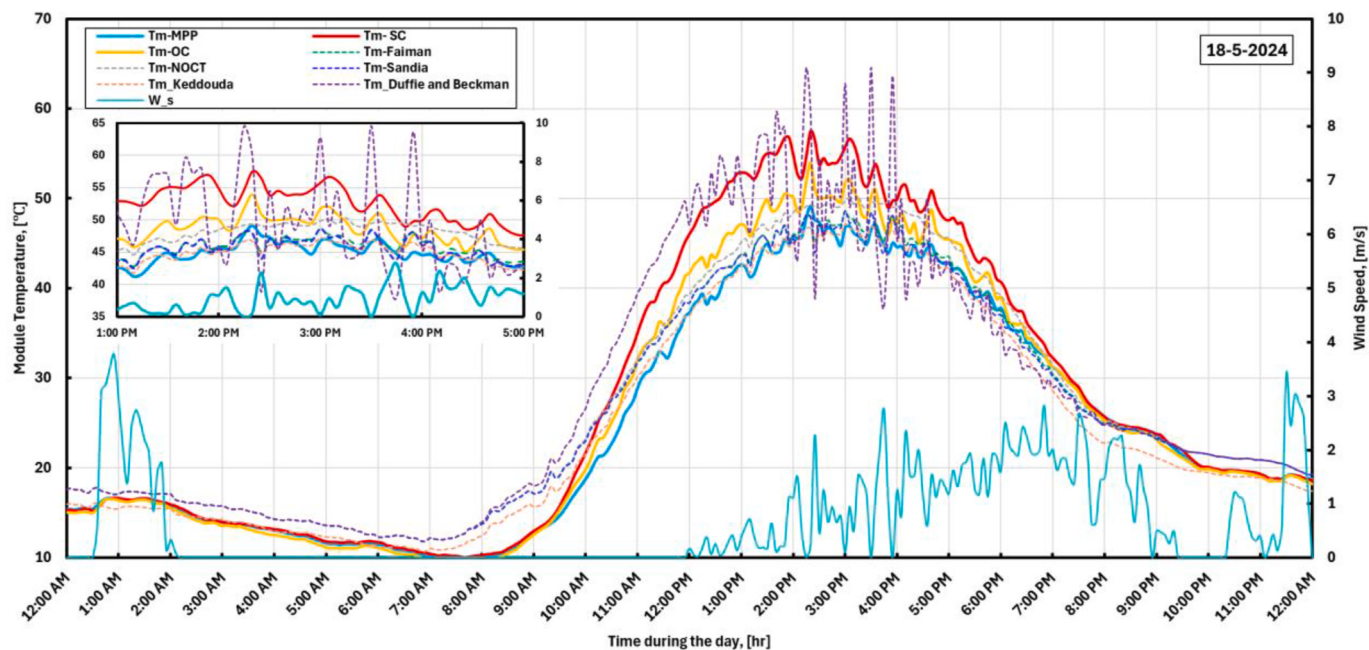


**Fig. 8.** Example of daily measured variables (5 min) time step: ambient variables (ambient temperature, wind speed, and POA irradiance) and PV module temperatures: measured at SC, OC, and MPP operating conditions and calculated by thermal models.

measured module temperature and the modeled one was considered during the 4 months of monitoring for short-circuited PV system MPP operated system, and open-circuited one as can be seen in Fig. 9. It worth mentioning that evaluating thermal models is preferred in clear sky steady conditions to avoid the miscalculation resulted from the delay in the thermal response.

The analysis reveals that the Faiman model, while considering  $\eta = 0$ , showed the best precision, relative to the other models examined, in estimating the short-circuited PV module with a daily monthly average temperature deviation between  $+2.72\text{ }^{\circ}\text{C}$  and  $-2.3\text{ }^{\circ}\text{C}$ , see Fig. 9-a. Moreover, the Keddouda model provides a high level of accuracy in estimating the module temperature operating at MPP status with an average daily overestimation of  $1.67\text{ }^{\circ}\text{C}$ . It can also be noticed that the examined thermal models tend to overestimate the module temperature that operates at MPP, as can be spotted in Fig. 9-b. This can be explained by the neglect of the thermal capacitance of the module itself and the lack of development of the proper thermal coefficients that acknowledge the new module technologies, their higher electrical efficiency, and installation solutions.

Both the Sandia and NOCT thermal models show better accuracy in estimating the temperature of an open-circuited PV module, with average overestimations of  $0.60\text{ }^{\circ}\text{C}$  and  $2.4\text{ }^{\circ}\text{C}$ , respectively. In contrast, for the PV module operating at MPP, the overestimations increase to  $2.67\text{ }^{\circ}\text{C}$  and  $4.48\text{ }^{\circ}\text{C}$ , respectively. This pattern is confirmed by the daily and monthly deviations observed during the monitoring period, as shown in Fig. 9-c. Duffie and Beckman provides the worst result in evaluating the module temperature considering the three electrical operating statuses with temperature overestimation reaches over than  $14\text{ }^{\circ}\text{C}$  on daily basis which is not recommended compared to the other models. Such evaluation was confirmed by the statistical analysis considering as can be seen in Fig. 10.

The deviations observed in April and June can be attributed to some instability and unpredictable weather conditions during these months. Specifically, April experienced significant rainfall, which aligns with the city's typical climate, characterized by wetter conditions in the spring. In contrast, June was much drier with warmer ambient temperatures, with average highs around  $30\text{ }^{\circ}\text{C}$ . The errors vary across thermal models due to their varying sensitivities to electrical operating conditions and

their responses to climatic variables. These factors—such as solar radiation, ambient temperature, and wind speed—have distinct impacts on the predicted module temperature, leading to greater deviations in certain months, especially when unexpected weather patterns occur.

A recalibration of the thermal model coefficients has been performed, taking into account the three examined electrical operating conditions. The coefficients for both the Faiman and Sandia thermal models were developed using separate datasets for a PV system operating under open-circuit, MPP, and short-circuit conditions, as shown in Table 4. A comparison with the literature coefficients for both models highlights the necessity of providing updated empirical coefficients for these conditions. Additionally, it underscores the lack of adaptability and the variation in accuracy relative to different electrical operating conditions.

#### 4.3. Thermal models sensitivity to the environmental variables

For a better insight into the thermal model's accuracy evaluation, the precision of the thermal models examined has been considered with respect to the various environmental variables that have a direct influence on the thermal behavior of the module temperature and, hence, the thermal model accuracy. The sensitivity of thermal models to key environmental variables—plane of array irradiance, ambient temperature, and wind speed—under different electrical operating conditions of the PV module is presented as follows.

##### • Precision assessment of irradiance sensitivity

Fig. 11 presents the error precision of the thermal models compared to the actual measurement of short-circuited PV modules (PV set-1). A clear underestimation can be noticed, especially for levels of radiation higher than  $300\text{ W/m}^2$ . An underestimation of up to 20 % has been found, especially in the Sandia and Keddouda models. On the other hand, the NOCT model achieved a better underestimation. Duffie and Beckman not only overestimated the module temperature at short circuit status but also suffered from multiple fluctuations for the same level of radiation relative to the corresponding wind speed considered.

When considering the evaluation of these thermal models against the

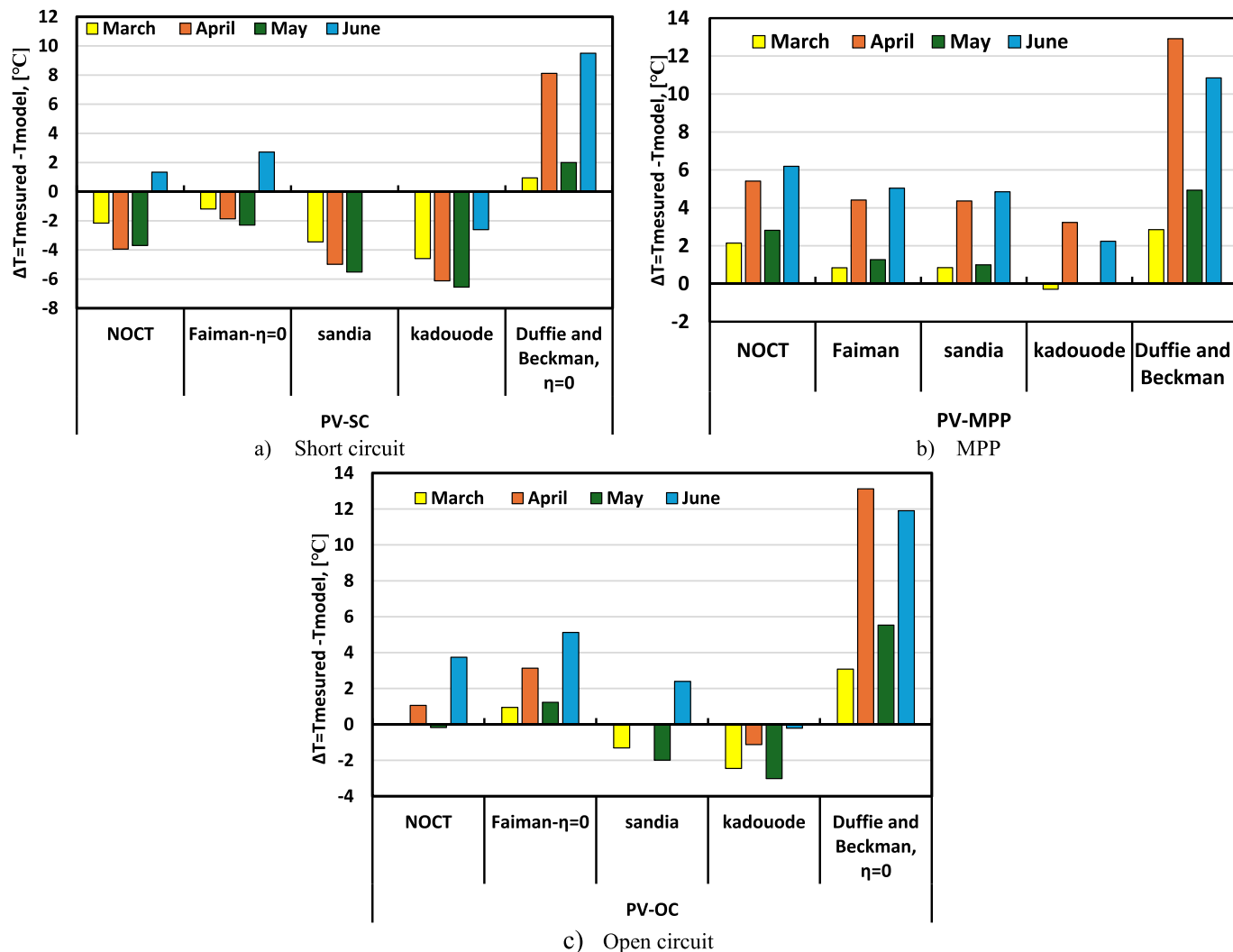


**Fig. 9.** The average monthly temperature difference between the measured and calculated module temperatures under different operational conditions: a) short-circuited PV system, b) PV system operating at maximum power point (MPP), and c) open-circuited PV system. The colors represent different months: yellow for March, orange for April, green for May, and blue for June. (For interpretation of the references to color in this figure legend, the reader is referred to the Web version of this article.)

temperature of an open-circuited PV module (PV set-2), see Fig. 12, a better precision can be noticed with a slight underestimation/overestimation precision ranging from  $-13\%$  to  $+10\%$ . After G<sub>POA</sub> of  $400 \text{ W/m}^2$ , the accuracy of the thermal models is very similar for higher levels of radiation, while the NOCT and Duffie and Beckman models tend to overestimate the open-circuited PV module temperature. As for the accuracy validation of these thermal models relative to the measured temperature of the PV module operating on MPP (PV set-3), see Fig. 13, the thermal models tend to overestimate the module temperature, especially for the low level of radiation G<sub>POA</sub>  $< 400 \text{ W/m}^2$ . Moreover, increasing the level of radiation has a positive impact on the precision of these models by around 20 %. Keddouda model has the best accuracy compared to other examined thermal models, especially for high levels of irradiance, as can be seen in Fig. 13.

The underestimation of the module temperature of the short-circuited PV module by these models can be referred to as the main assumption adopted by the models that take into account a part of the received radiation is lost from the system in the form of electrical energy; nevertheless, the internal resistance of the cells itself that worked as an internal heat source. The better precision in estimating the open-circuited PV module temperature can be explained by the fact that these models assume the PV module behaves like a flat plate solar

collector. Additionally, the electrical efficiency used in their formulas to estimate the coefficients was much lower compared to modern modules. Furthermore, these thermal models lack clear information about the electrical connection status of the examined PV module. As a result, the models tend to overestimate the temperature of the module operating at MPP.

Analyzing the available records taken during the 4 months of monitoring according to grouped levels of irradiance is presented in Fig. 14. Such analysis reveals that around 40 % of the available irradiance records are below  $300 \text{ W/m}^2$ , while high levels of irradiance between  $700$  and  $1100 \text{ W/m}^2$  represents about 38 % of the database.

The mean of thermal models' precision for grouped levels of irradiance can give a better comprehension of the impact of the irradiance sensitivity considering different electrical operating statuses. The percentage deviation of thermal model predictions from experimentally measured PV module temperatures across the plane of array irradiance ranges ( $< 100$ – $1100 \text{ W/m}^2$ ) and electrical operating conditions (short-circuit, maximum power point operation, and open-circuit) is presented in Fig. 15 a, b, and c respectively. Positive deviations indicate overestimation of temperature, while negative values reflect underestimation. This analysis explores the performance of five models—Duffie and Beckman, NOCT, Faiman, Sandia, and Keddouda—under these varying

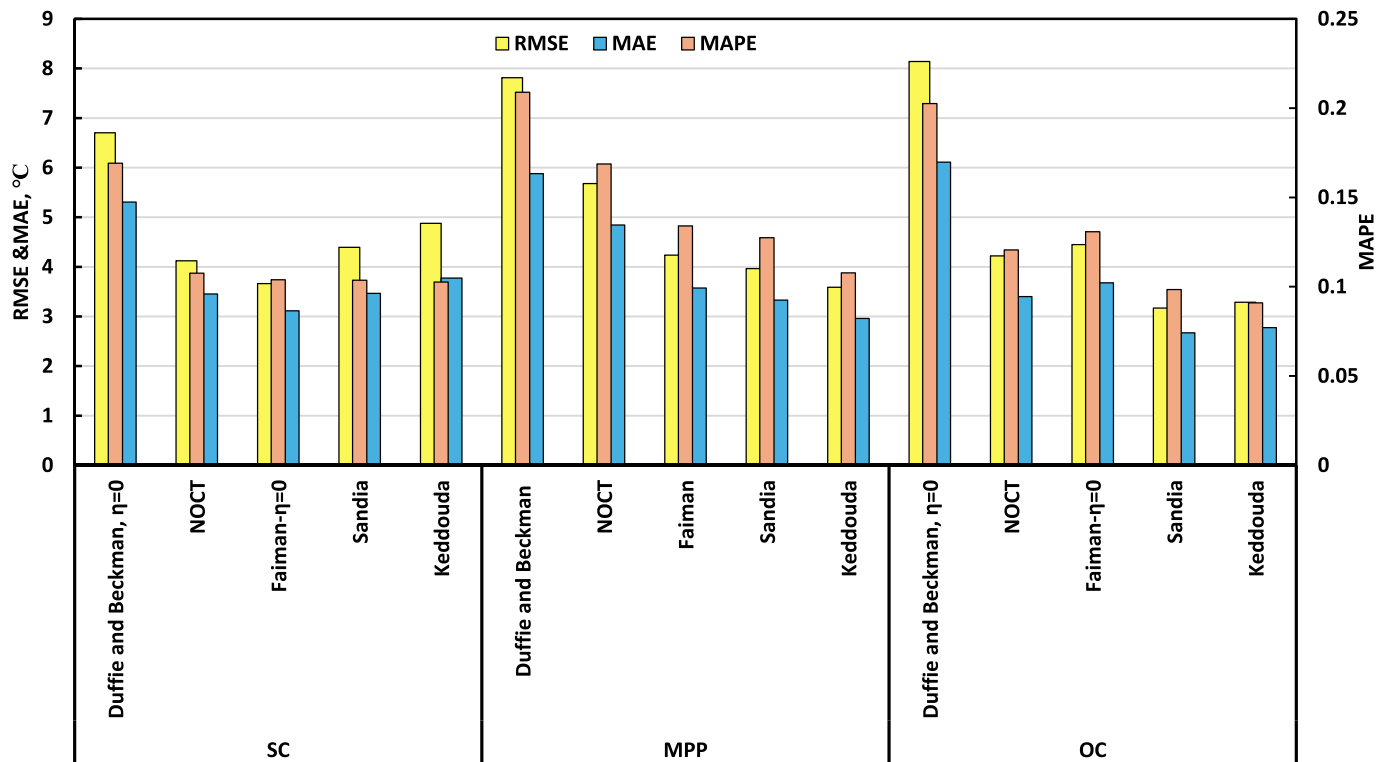


Fig. 10. Statistical analysis of the thermal models for the different electrical operating statuses.

**Table 4**  
Optimized thermal coefficients of different extreme electrical operating conditions.

| Thermal model   |     | Thermal coefficients    |                           |
|-----------------|-----|-------------------------|---------------------------|
| Faiman model    |     | Uc W/m <sup>2</sup> ·°C | Uv W.s/m <sup>3</sup> ·°C |
| Present work    | MPP | 33.1848                 | 2.2733                    |
|                 | OC  | 26.204                  | 3.4028                    |
|                 | SC  | 22.3035                 | 3.1976                    |
| Literature [27] |     | 25                      | 1.2                       |
|                 | a   | b                       |                           |
| Sandia model    | MPP | -3.7448                 | -0.0646                   |
|                 | OC  | -3.5123                 | -0.1128                   |
|                 | SC  | -3.3535                 | -0.1214                   |
| Literature [26] |     | -3.56                   | -0.075                    |

scenarios.

It can be seen in Fig. 15-a for short-circuited PV that increasing the level of irradiance improves the accuracy of NOCT and Faiman- $\eta = 0$  thermal models (1.71 % and 3.48 %, respectively, for irradiance between 700 and 900W/m<sup>2</sup>). Yet Sandia and Keddouda's models tend to underestimate the short-circuited system, especially for high levels of radiation.

It can be seen in Fig. 15-b that all examined thermal models tend to overestimate the temperature of a PV module operating in MPP for all levels of radiation. The Keddouda model has the highest precision for all levels of irradiance examined compared to the other mentioned models. Yet For low levels of radiation (100–300 W/m<sup>2</sup>), the accuracy of the Duffie and Beckman model is around 24.39 %. The accuracy of both Sandia and Faiman has a similar response of around 10 % for levels of radiation >300W/m<sup>2</sup>. NOCT model has a similar accuracy of around 15 % for all different levels of irradiance.

The radiation sensitivity of the thermal model accuracy in estimating the open-circuited PV module temperature is presented in Fig. 15-c. It can be seen that for lower levels of radiation of 300W/m<sup>2</sup>, the mentioned models tend to have a low precision between 15 % and 18 %,

yet Keddouda provides an improved evaluation from 9.45 % to 2.45 %. On the other hand, with a higher level of irradiance of 300 W/m<sup>2</sup>, both Keddouda and Sandia tend to underestimate the open-circuited module with a reasonable level of accuracy that doesn't exceed  $\pm 2.6$  %. Both Faiman- $\eta = 0$  and NOCT models follow the same pattern of increasing their accuracy of anticipating open-circuited PV module temperature with increasing the level of radiation>300 W/m<sup>2</sup>.

#### • Precision assessment of ambient temperature sensitivity

Ambient temperature is a crucial environmental factor that directly influences the increase in module temperature. Although the examined thermal models assign a unity coefficient to ambient temperature, its sensitivity can vary across different models and electrical operating conditions. An analysis of the ambient temperature values in the available dataset, as shown in Fig. 16, reveals that temperatures between 20 and 25 °C account for approximately 50 % of the recorded measurements. In contrast, only 6 % of the dataset corresponds to ambient temperatures lower than 15 °C.

Fig. 17 depicts the percentage deviation of thermal model predictions from experimentally measured PV module temperatures across ambient temperature ranges (5–30 °C) and electrical operating conditions (short-circuit, maximum power point operation, and open-circuit). Positive deviations indicate overestimation of temperature, while negative values reflect underestimation. This analysis explores the performance of five models—Duffie and Beckman, NOCT, Faiman, Sandia, and Keddouda—under these varying scenarios.

Generally, it can be observed that, regardless of the electrical operating conditions, all examined thermal models exhibit very low accuracy at low ambient temperatures ( $5^{\circ}\text{C} < T_{\text{m}} < 10^{\circ}\text{C}$ ), which typically occur during the early morning hours. Increasing the ambient temperature has a positive impact on the accuracy of the thermal models, see Fig. 17. When the PV system is operating in short circuit conditions, the precision deviation of Duffie and Beckman reduced from 79 % at ( $T_{\text{amb}} = 5\text{--}10^{\circ}\text{C}$ ) to around 1 % at ( $T_{\text{amb}} = 25\text{--}30^{\circ}\text{C}$ ), see Fig. 17-a. Both NOCT

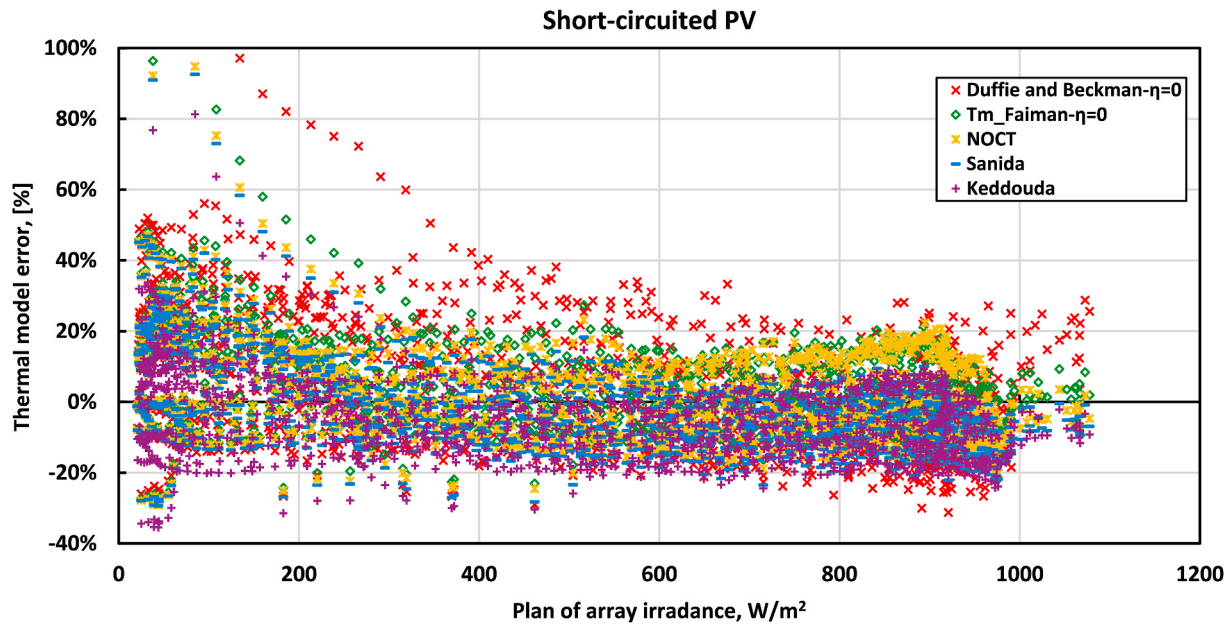


Fig. 11. Thermal model precision relative to short-circuited PV module (PV set 1).

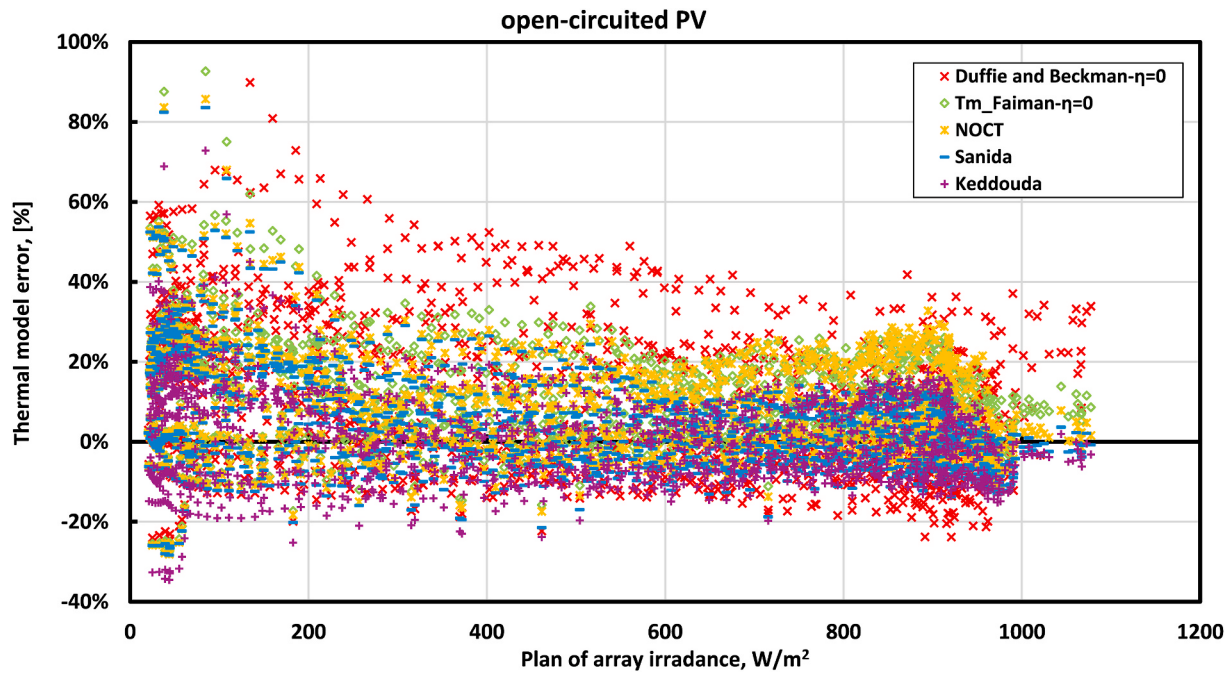


Fig. 12. Thermal model precision relative to open-circuited PV module (PV set 2).

and Faiman models have the same performance pattern that achieved high precision with minimum deviation, 2 %, and 3 %, respectively, from the measured short-circuited PV module temperature at  $T_{amb} = 25\text{--}30\text{ }^{\circ}\text{C}$ . Moreover, Sandia and Keddouda have an underestimation prediction for  $T_{amb} < 15\text{ }^{\circ}\text{C}$ .

Thermal modeling of an MPP operating system can achieve a high level of accuracy with the Keddouda model, particularly at high ambient temperatures ( $T_{amb} = 25\text{--}30\text{ }^{\circ}\text{C}$ ); see Fig. 17-b. On the other hand, the Duffie and Beckman model exhibits the worst performance, with an error estimation of approximately 96 % at low ambient temperatures ( $T_{amb} = 5\text{--}10\text{ }^{\circ}\text{C}$ ). Both Faiman and Sandia models exhibit a similar error pattern, with accuracy improving as ambient temperature increases, reducing the estimation error from 53 % to 8 % for  $T_{amb} = 5\text{--}30\text{ }^{\circ}\text{C}$ .

Similarly, the NOCT model shows comparable performance, with its estimation error decreasing from 55 % to 11 % over the same temperature range.

Under open-circuit conditions, where no electrical current flows, thermal models generally exhibit higher deviations at lower ambient temperatures  $T_{amb} = 5\text{--}15\text{ }^{\circ}\text{C}$ . Although the Duffie and Beckman model shows a 72 % deviation in this temperature range, indicating unaccounted variables such as convective cooling or irradiance effects, it achieves a highly accurate estimation with only a 3 % error at  $T_{amb} = 20\text{--}25\text{ }^{\circ}\text{C}$ . Both the NOCT and Faiman models follow a similar performance pattern, achieving high precision with minimal deviations of 7 % and 9 %, respectively, from the measured open-circuit PV module temperature at  $T_{amb} = 20\text{--}25\text{ }^{\circ}\text{C}$ . Furthermore, the Keddouda model,

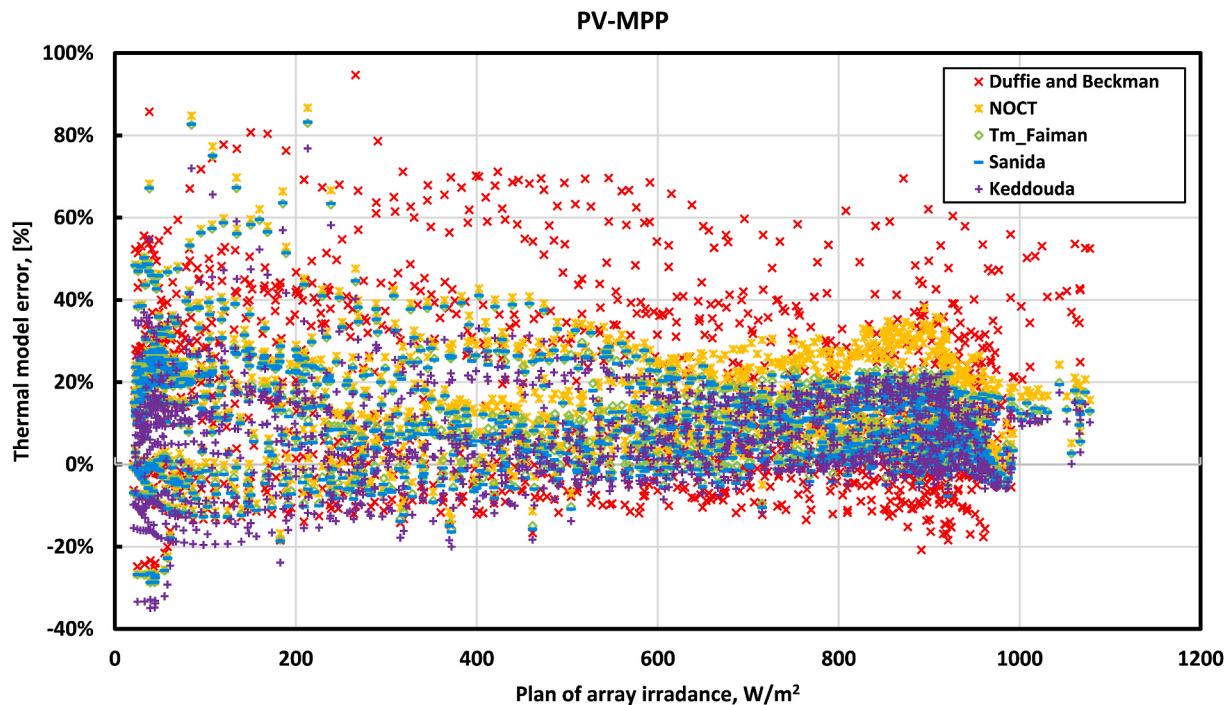


Fig. 13. Thermal model precision relative to PV module operate at MPP, (PV set 3).

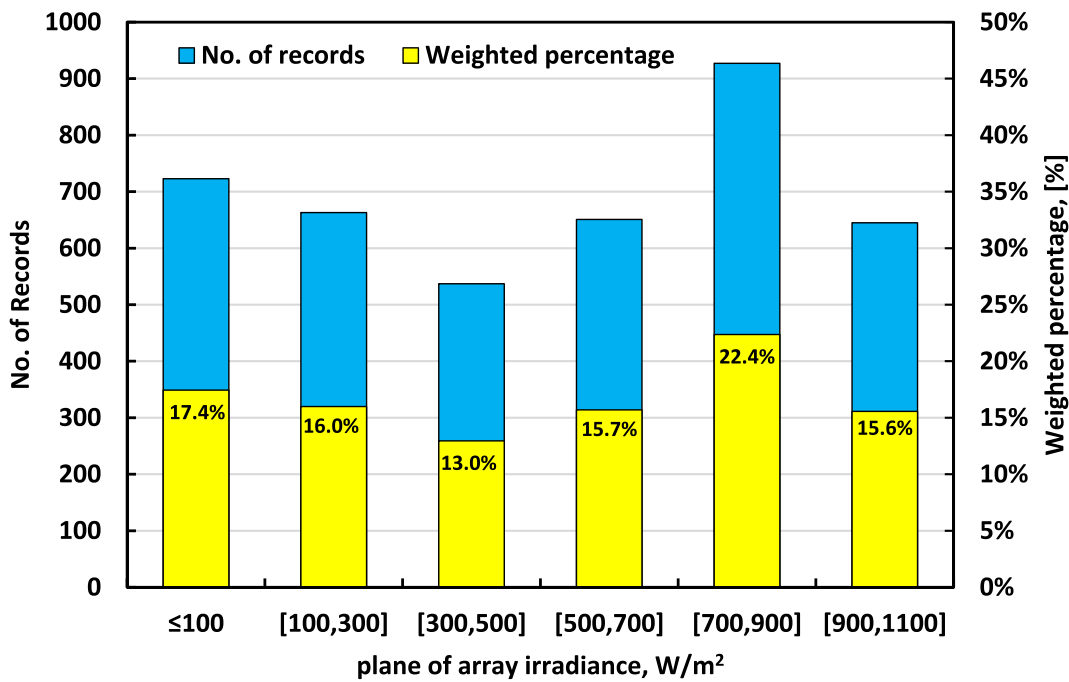


Fig. 14. Statistical analysis of the dataset according to irradiance ranges.

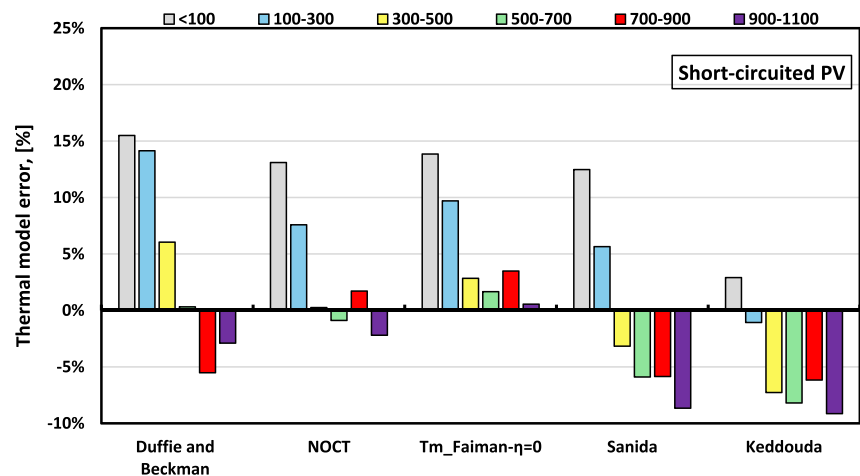
remaining the most stable, demonstrates the best estimation accuracy among all examined thermal models, with its overestimation error decreasing from 29 % at low ambient temperatures to an underestimation error of just 1 % at ( $T_{amb} = 20\text{--}30\text{ }^{\circ}\text{C}$ ).

Thermal model accuracy is highly sensitive to ambient temperature and electrical operating conditions. In temperate climates (5–15 °C), the Keddouda model is the optimal choice, particularly for open-circuit or MPP systems. In hotter regions (25–30 °C), both the Keddouda and Sandia models are indispensable, while models like Duffie and Beckman should be avoided due to their tendency for risky overestimation. These

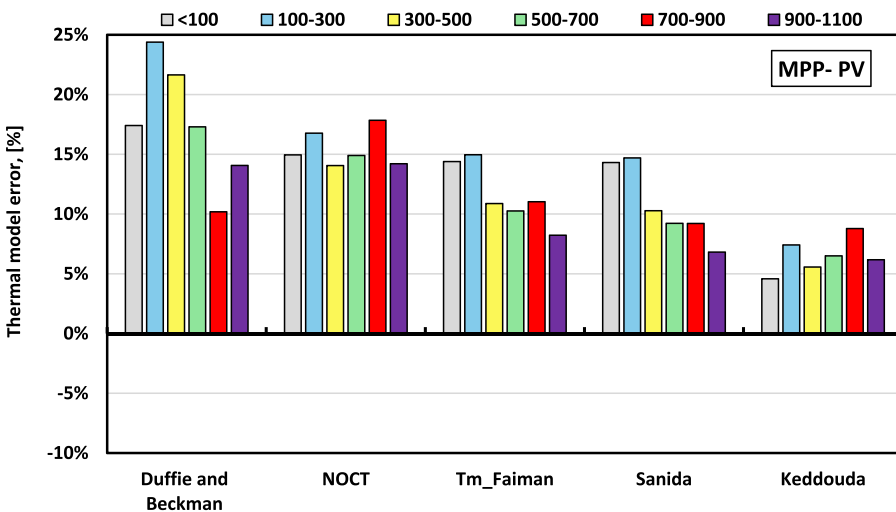
findings highlight the importance of context-aware model selection and the need for empirical frameworks validated against real-world operating data.

#### • Precision assessment of wind speed sensitivity

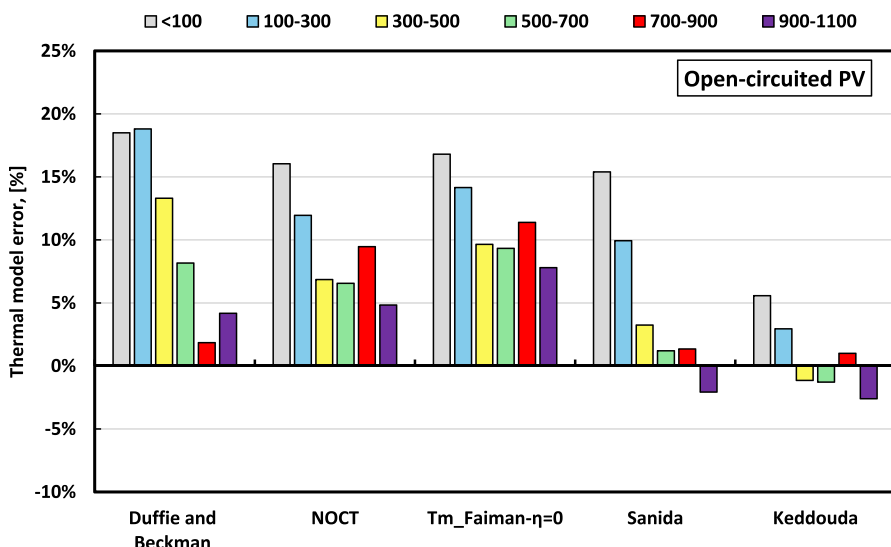
While wind speed has a decreasing influence on module temperature, the sensitivity of each thermal model varies significantly depending on the electrical operating conditions, making it an essential factor to investigate. Based on the available dataset, a wind speed distribution



a) Short-circuited PV



b) PV-MPP



c) Open-circuited PV

**Fig. 15.** Average thermal models precision for wide levels of radiation considering different PV electrical operation statuses: a) Short-circuited PV, b) PV-MPP, and c) Open-circuited PV.

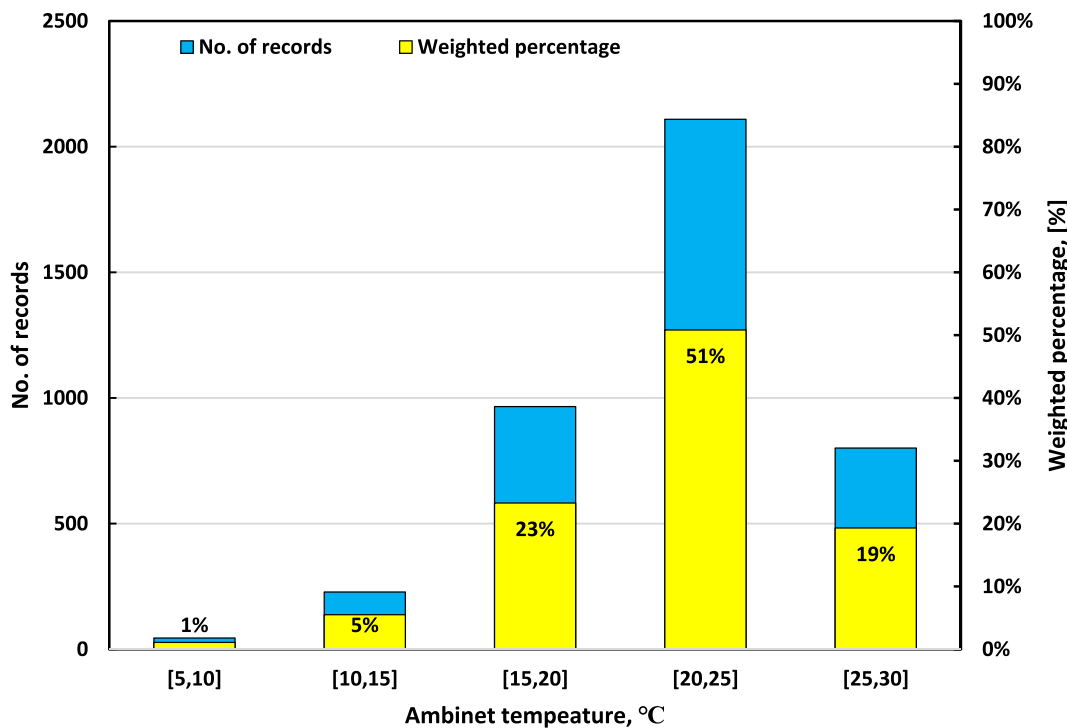


**Fig. 16.** Statistical analysis of the dataset according to ambient temperature ranges.

has been introduced along with its weighted percentage to provide better insight, as shown in Fig. 18. The data reveals that stagnant wind conditions were predominant at the experimental location, with approximately 55 % of recorded values around 1 m/s. In contrast, only 5 % of the dataset includes wind speeds in the range of 3–5 m/s.

The sensitivity of the examined thermal models to wind speed under different electrical operating conditions is shown in Fig. 19. When the PV system operates under short-circuit conditions (Fig. 19-a), the Duffie and Beckman model tends to underestimate the module temperature by 5–23 % for high wind speeds (1–5 m/s). In contrast, the NOCT model, which does not account for wind speed, overestimates the temperature by up to 12 %. The Faiman model shows an average overestimation of approximately 5–7.5 % for wind speeds between 0 and 5 m/s. The Sandia model generally underestimates the module temperature by 3–5.6 % for wind speeds between 1 and 5 m/s, although it achieves high precision at wind speeds below 1 m/s.

The thermal models tend to overestimate the module temperature under maximum power point (MPP) conditions (Fig. 19-b). However, the Duffie and Beckman model shows underestimation in the range of 2–13 % for wind speeds of 2–5 m/s, while it significantly overestimates the temperature at wind speeds below 1 m/s. This variation in performance highlights the model's high sensitivity to wind speed. The NOCT model demonstrates a significant overestimation of 10–26 % at higher wind speeds. Both the Faiman and Sandia models exhibit similar overestimation trends, with the Sandia model showing slightly better accuracy.

Among the examined thermal models, the Keddouda model generally provides accurate modeling performance, particularly at wind speeds of 1–2 m/s, where it achieves an accuracy deviation of just 1.38 %. However, for the Keddouda model, increasing wind speed negatively impacts the accuracy of module temperature predictions when the PV system operates at maximum power point (MPP) conditions, as observed in Fig. 19-b.

In the case of open-circuited PV systems, the behavior is similar to that observed in MPP and short-circuit conditions. The Duffie and Beckman model tends to underestimate the module temperature by 0.5–17 % as wind speed increases from 1 to 5 m/s (Fig. 19-c). On the

other hand, the Sandia model demonstrates better accuracy in modeling the module temperature of an open-circuited PV system, with an error ranging from 6 % to 2 % as wind speed increases from 0 to 5 m/s. The NOCT model shows an overestimation deviation of approximately 6–21 % as wind speed increases from 1 to 5 m/s, while the Keddouda model presents a more moderate overestimation deviation, ranging from 3.5 % to 7 %.

## 5. Conclusion

The evaluation of the impact of the electrical operation conditions on the thermal performance of a rooftop monofacial PV system is conducted in the present work. During four months, the thermal performances of three PV sets, each operating in different statuses: short-circuited (PV set-1), open-circuited (PV set-2), and maximum power point (MPP) (PV set-3) have been monitored, and the recorded data analyzed. PV module thermal models alongside their commonly cited coefficients, namely the Faiman model, NOCT model, Sandia model, Duffie and Beckman model, and Keddouda model have been evaluated against the different electrical operating statuses. Furthermore, a sensitive evaluation of these thermal models against different levels of irradiance is performed for better insight. In summary, the current work developed the following observations:

Thermal performance of the PV module temperature at different electrical operating conditions.

- Depending on the received irradiance and ambient conditions, the average daily temperature of a short-circuited PV module is 4.30 °C–9.35 °C higher than that of a module operating at MPP.
- The temperature of an open-circuited PV module is elevated by 2.16 °C–4.35 °C which is approximately 8.01 % higher compared to an MPP-operating system.
- Short-circuited PV modules develop multiple hotspots, posing a significant risk to module health.
- Open-circuited PV modules exhibit a more uniform but elevated temperature distribution relative to the system operating at MPP.

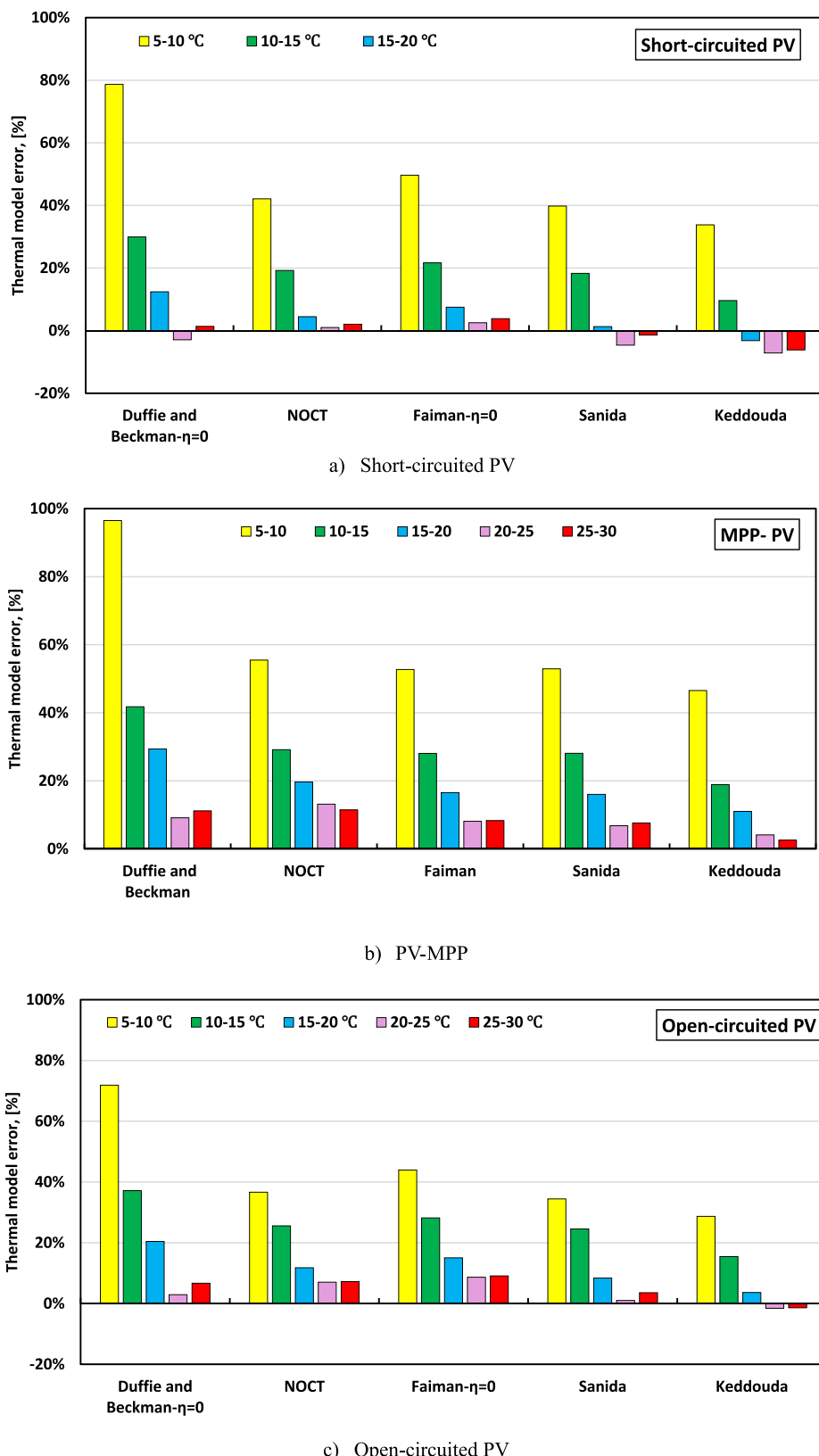


**Fig. 17.** Average thermal models precision for various ambient temperature levels considering different PV electrical operation statuses: a) Short-circuited PV, b) PV-MPP, and c) Open-circuited PV.

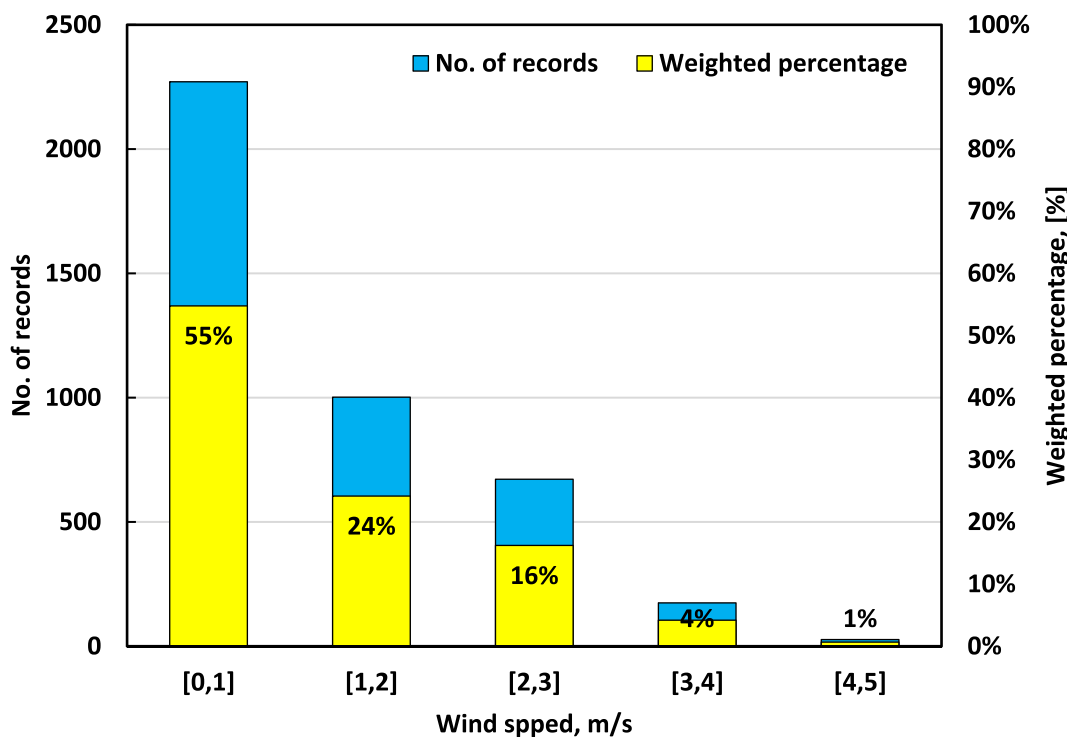


**Fig. 18.** Statistical analysis of the dataset according to ambient temperature ranges.

Thermal models performance for short-circuited PV systems.

- The Faiman model (with  $\eta = 0$ ) and the NOCT model demonstrate relatively high precision in estimating short-circuited PV module temperatures, with an underestimation of 1–2 °C.
- Under short-circuit conditions, most models tend to underestimate temperatures. The Duffie and Beckman model underestimates by 5–23 % at high wind speeds, while the NOCT model tends to overestimate by up to 12 %.

Thermal models performance for (MPP) Operation.

- The Keddouda model demonstrates the highest precision in estimating MPP module temperature, with a mean deviation of less than 3 %. Its accuracy improves at higher irradiance levels.
- The NOCT model tends to overestimate the module temperature at MPP by an average of 15.33 %, while the Faiman model overestimates by 16.65 %.
- Most thermal models overestimate module temperature. However, the Duffie and Beckman model behaves differently, underestimating at higher wind speeds (2–5 m/s) and overestimating at lower wind speeds (<1 m/s).

Thermal model performance for open-circuited PV systems.

- The Sandia model provides the closest estimation of open-circuit module temperature, with an RMSE of 3.17 °C and an MAE of 2.19 °C.
- At lower irradiance levels ( $300 \text{ W/m}^2$ ), most models exhibit low precision, with errors ranging between 15 % and 18 %. The Keddouda model demonstrates improved accuracy, reducing errors from 9.45 % to 2.45 %. At higher irradiance levels ( $>300 \text{ W/m}^2$ ), both the Keddouda and Sandia models tend to slightly underestimate the open-circuited module temperature but maintain a reasonable accuracy within  $\pm 2.6 \%$ .

Effect of environmental conditions on the thermal model's accuracy.

- As ambient temperature increases, model accuracy improves, with significantly reduced errors for all models at  $T_a = 25\text{--}30^\circ\text{C}$ .
- The Duffie and Beckman model exhibits high sensitivity to wind speed, leading to large fluctuations and temperature deviations of up to 15–20 °C, regardless of the system's electrical operating status.
- The Keddouda model provides the most accurate predictions at wind speeds of 1–2 m/s but loses accuracy as wind speed increases.
- The Sandia model demonstrates better accuracy for open-circuited PV systems.

Recommendations for different climates.

- In temperate climates (5–15 °C), the Keddouda model is recommended due to its superior accuracy. While in hotter conditions (25–30 °C), both the Keddouda and Sandia models provide reliable temperature predictions.
- The Keddouda model is the most stable and accurate across different conditions, particularly at higher temperatures.

Accordingly, improving existing thermal models and their recalibrating empirical coefficients for different electrical operating conditions is crucial—not only for the reliable monitoring of a healthy PV system operating at maximum power point (MPP) conditions but also for enhancing their sensitivity to different electrical operating states. Future work will focus on refining thermal models to incorporate input data related to the system's electrical operating point. This advancement will provide deeper insights and more accurate modeling for monitoring and assessing system performance.

#### CRediT authorship contribution statement

**Amr Osama:** Data curation, Formal Analysis, Investigation, Software, Validation, Writing – original draft. **Giuseppe Marco Tina:** Writing – review & editing, Supervision, Resources, Project administration, Methodology, Investigation, Funding acquisition, Formal analysis, Conceptualization. **Antonio Gagliano:** Writing – review & editing, Supervision, Methodology, Investigation, Formal analysis,

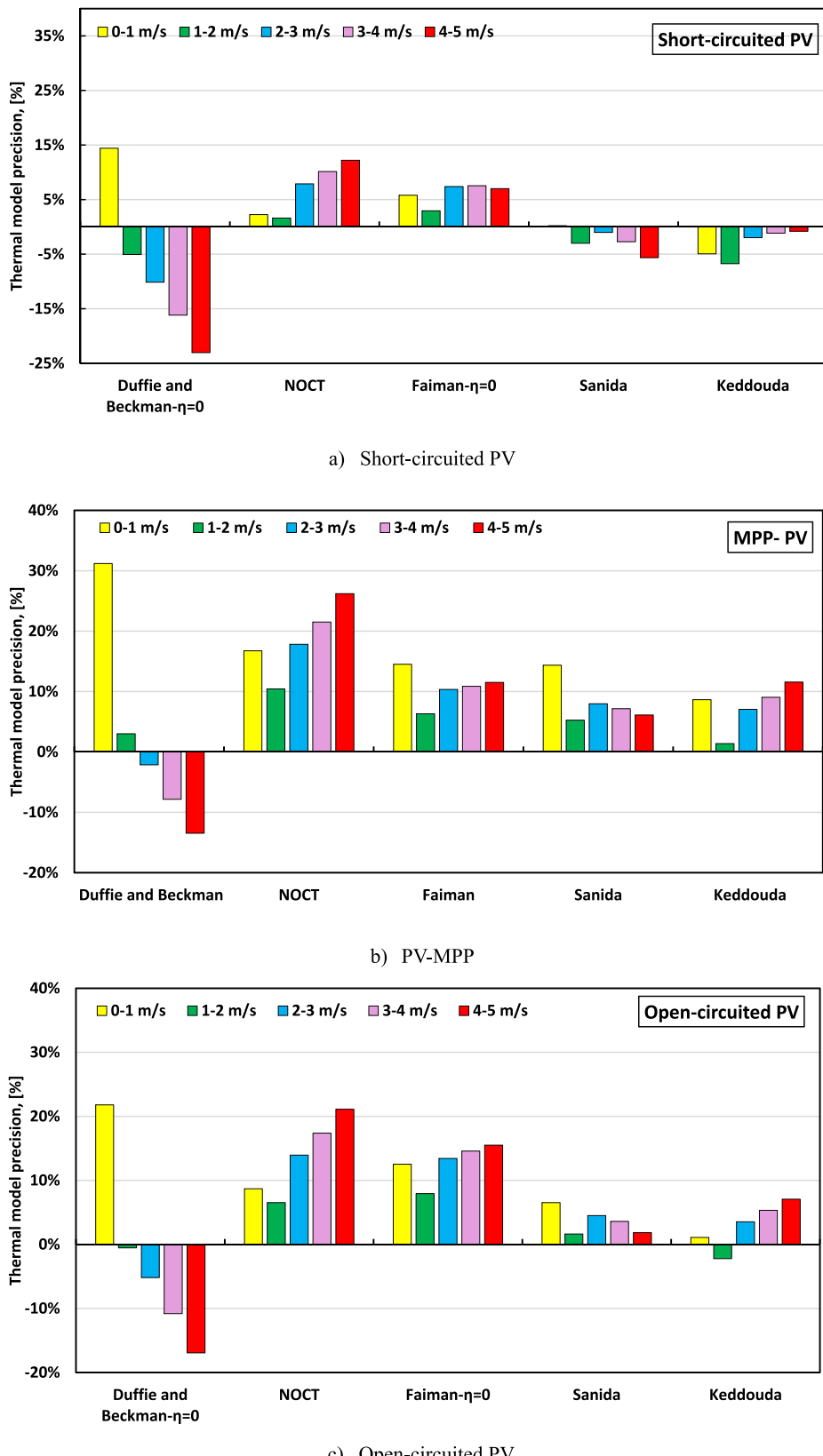


**Fig. 19.** Average thermal models precision for various wind speed levels considering different PV electrical operation statuses: a) Short-circuited PV, b) PV-MPP, and c) Open-circuited PV.

Conceptualization. **Gabino Jimenez-Castillo:** Writing – review & editing, Methodology, Investigation, Formal analysis, Data curation. **Francisco José Munoz-Rodríguez:** Writing – review & editing, Resources, Project administration, Methodology, Formal analysis, Conceptualization.

### Declaration of competing interest

The authors declare the following financial interests/personal relationships which may be considered as potential competing interests.

### Acknowledgment

This work has been supported by the Italian National Ph.D. in Photovoltaics, CURRICULUM C: Monitoring and Diagnosis has been received. Also, support by MUR, Italy funds in the frame of PRIN 2020 “A Holistic Monitoring and Diagnostic Tool for Photovoltaic Generators (HOTSPHOT)” project (CUP:E63C2001116000) and Grant TED2021-131137B-I00 “Aportación a la Transición Ecológica en el sector Industrial a través del Autoconsumo Fotovoltaico” funded by MICIU/AEI/10.13039/501100011033 and European Union Next Generation EU/PRTR.

### Data availability

Data will be made available on request.

### References

- [1] EU commission, EU commission Fit for 55 package. <https://www.consilium.europa.eu/en/policies/fit-for-55/>, 2023. (Accessed 18 December 2024).
- [2] IEA, Renewables 2024 analysis and forecast to 2030. <https://www.iea.org/reports/renewables-2024>, 2024.
- [3] IEA, Renewable Energy Market Update, 2024.
- [4] IEA, Renewable Electricity Capacity Additions by Technology and Segment, 2016–2028, IEA, Paris, 2024. <https://www.iea.org/data-and-statistics/charts/renewable-electricity-capacity-additions-by-technology-and-segment-2016-2028>. Licence: CC BY 4.0.
- [5]IRENA, Renewable Generation Costs in 2023, 2024.
- [6] M.S. Chowdhury, K.S. Rahman, T. Chowdhury, N. Nuthammachot, K. Techato, M. Akhtaruzzaman, S.K. Tiong, K. Sopian, N. Amin, An overview of solar photovoltaic panels' end-of-life material recycling, *Energy Strategy Rev.* 27 (2020) 100431, <https://doi.org/10.1016/j.esr.2019.100431>.
- [7] A. Allouhi, S. Rehman, M.S. Buker, Z. Said, Up-to-date literature review on Solar PV systems: technology progress, market status and R&D, *J. Clean. Prod.* 362 (2022) 132339, <https://doi.org/10.1016/j.jclepro.2022.132339>.
- [8] R. Aman, M. Rizwan, A. Kumar, Fault classification using deep learning based model and impact of dust accumulation on solar photovoltaic modules, *Energy Sources, Part A Recover. Util. Environ. Eff.* 45 (2023) 4633–4651, <https://doi.org/10.1080/15567036.2023.2205859>.
- [9] IEA-PVPS, Guidelines for operation and maintenance of photovoltaic power plants in different climates 2022 PVPS task 13 reliability and performance of photovoltaic systems. <https://iea-pvps.org/research-tasks/performance-operation-and-reliability-of-photovoltaic-systems/>, 2022.
- [10] A. Ziane, R. Dabou, A. Necibaia, N. Sahouane, M. Mostefaoui, A. Bouraiou, S. Khelifi, A. Rouabchia, M. Blal, Tree-based ensemble methods for predicting the module temperature of a grid-tied photovoltaic system in the desert, *Int. J. Green Energy* 18 (2021) 1430–1440, <https://doi.org/10.1080/15435075.2021.1904945>.
- [11] N. Bailek, K. Bouchouicha, M.A. Hassan, A. Slimani, B. Jamil, Implicit regression-based correlations to predict the back temperature of PV modules in the arid region of south Algeria, *Renew. Energy* 156 (2020) 57–67, <https://doi.org/10.1016/j.renene.2020.04.073>.
- [12] K. Kouame, D. Danovitch, P. Albert, A. Turala, M. Volatier, V. Aimez, A. Jaouad, M. Darnon, G. Hamon, Finite element modeling and experimental validation of concentrator photovoltaic module based on surface Mount technology, *Sol. Energy Mater. Sol. Cells* 272 (2024) 112890, <https://doi.org/10.1016/j.solmat.2024.112890>.
- [13] M. Prilliman, J.S. Stein, D. Riley, G. Tamizhmani, Transient weighted moving-average model of photovoltaic module back-surface temperature, *IEEE J. Photovoltaics* 10 (2020) 1053–1060, <https://doi.org/10.1109/JPHOTOV.2020.2992351>.
- [14] R. Aalloul, R. Adhiri, M. Benlattar, A. Elaissaoui, Coupled electrical–thermal modeling of photovoltaic modules: an overview, *Therm. Sci. Eng. Prog.* 55 (2024) 102962, <https://doi.org/10.1016/j.tsep.2024.102962>.
- [15] D. Torres Lobera, S. Valkealahti, Dynamic thermal model of solar PV systems under varying climatic conditions, *Sol. Energy* 93 (2013) 183–194, <https://doi.org/10.1016/j.solener.2013.03.028>.
- [16] R. Korab, M. Polomski, T. Naczynski, T. Kandzia, A dynamic thermal model for a photovoltaic module under varying atmospheric conditions, *Energy Convers. Manag.* 280 (2023) 116773, <https://doi.org/10.1016/j.enconman.2023.116773>.
- [17] C. Li, S.V. Spataru, K. Zhang, Y. Yang, H. Wei, A multi-state dynamic thermal model for accurate photovoltaic cell temperature estimation, *IEEE J. Photovoltaics* 10 (2020) 1465–1473, <https://doi.org/10.1109/JPHOTOV.2020.2987401>.
- [18] G.M. Tina, F.B. Scavo, A. Gagliano, Multilayer thermal model for evaluating the performances of monofacial and bifacial photovoltaic modules, *IEEE J. Photovoltaics* 10 (2020) 1035–1043.
- [19] L. de O. Santos, P.C.M. de Carvalho, C. de O.C. Filho, Photovoltaic cell operating temperature models: a review of correlations and parameters, *IEEE J. Photovoltaics* 12 (2022) 179–190, <https://doi.org/10.1109/JPHOTOV.2021.3113156>.
- [20] R. Korab, M. Polomski, T. Naczynski, T. Kandzia, A dynamic thermal model for a photovoltaic module under varying atmospheric conditions, *Energy Convers. Manag.* 280 (2023) 116773, <https://doi.org/10.1016/j.enconman.2023.116773>.
- [21] N. Aoun, Methodology for predicting the PV module temperature based on actual and estimated weather data, *Energy Convers. Manag.* X 14 (2022) 100182, <https://doi.org/10.1016/j.ecmx.2022.100182>.
- [22] E. Barykina, A. Hammer, Modeling of photovoltaic module temperature using Faiman model: sensitivity analysis for different climates, *Sol. Energy* 146 (2017) 401–416, <https://doi.org/10.1016/j.solener.2017.03.002>.
- [23] D.L. King, W.E. Boyson, J.A. Kratochvil, Photovoltaic array performance model 8 (2004) 1–19.
- [24] G. Osma-Pinto, G. Ordóñez-Plata, Dynamic thermal modelling for the prediction of the operating temperature of a PV panel with an integrated cooling system, *Renew. Energy* 152 (2020) 1041–1054, <https://doi.org/10.1016/j.renene.2020.01.132>.
- [25] T.W. Neises, S.A. Klein, D.T. Reindl, Development of a thermal model for photovoltaic modules and analysis of NOCT guidelines, *J. Sol. Energy Eng. Trans. ASME* 134 (2012) 1–7, <https://doi.org/10.1115/1.4005340>.
- [26] D.L. King, W.E. Boyson, J.A. Kratochvil, Photovoltaic array performance model, 1–19, <https://doi.org/10.2172/919131>, 2004.
- [27] PVsyst Array Thermal losses, (n.d.). <https://www.pvsyst.com/help/project-design/array-and-system-losses/array-thermal-losses/index.html>.
- [28] P. Gilman, A. Dobos, N. DiOrio, J. Freeman, S. Janzou, D. Ryberg, System advisor model (SAM) photovoltaic model technical reference update, *Natl. Renew. Energy Lab* (2018) 93. [https://sam.nrel.gov/images/web\\_page\\_files/sam-help-2018-11-11-r4.pdf%0Asam.nrel.gov/content/downloads](https://sam.nrel.gov/images/web_page_files/sam-help-2018-11-11-r4.pdf%0Asam.nrel.gov/content/downloads).
- [29] K. Ardaní, P. Denholm, T. Mai, R. Margolis, T. Silverman, J. Zuboy, Solar futures study, U S Dep. Energy (2021) 1–279.
- [30] B.L. Smith, M. Woodhouse, K.A.W. Horowitz, T.J. Silverman, J. Zuboy, R. Margolis, Photovoltaic (PV) Module Technologies : 2020 Benchmark Costs and Technology Evolution Framework Results, National Renewable Energy Laboratory, Golden, CO, 2021. NREL/TP-7A40-78173.
- [31] D. Philips, W. Warmuth, Photovoltaics report. [www.ise.fraunhofer.de](http://www.ise.fraunhofer.de), 2021.
- [32] L. Haas, F.C. Cavalcanti, C.K.F. Da Silva, Parametric sensitivity analysis of a one-dimensional thermal-electrical model of a photovoltaic solar module, *Obs. La Econ. Latinoam* 21 (2023) 14346–14368, <https://doi.org/10.55905/oelv21n9-206>.
- [33] A. Ataman, N. Arslanoglu, Investigation of the cooling effect of wind on rooftop PV power plants, *Case Stud. Therm. Eng.* 63 (2024) 1–15, <https://doi.org/10.1016/j.csite.2024.105295>.
- [34] J.M. Servant, CALCULATION OF THE CELL TEMPERATURE FOR PHOTOVOLTAIC MODULES FROM CLIMATIC DATA 3 (1986) 1640–1643, <https://doi.org/10.1016/B978-0-08-033177-5.50311-2>.
- [35] M. Mattei, G. Notton, C. Cristofari, M. Muselli, P. Poggi, Calculation of the polycrystalline PV module temperature using a simple method of energy balance, *Renew. Energy* 31 (2006) 553–567, <https://doi.org/10.1016/j.renene.2005.03.010>.
- [36] J.D. Mondol, Y.G. Yohanis, B. Norton, Comparison of measured and predicted long term performance of grid connected photovoltaic system, *Energy Convers. Manag.* 48 (2007) 1065–1080, <https://doi.org/10.1016/j.enconman.2006.10.021>.
- [37] S. Pereira, P. Canhoto, T. Oozeki, R. Salgado, Assessment of thermal modeling of photovoltaic panels for predicting power generation using only manufacturer data, *Energy Rep.* 12 (2024) 1431–1448, <https://doi.org/10.1016/j.egyr.2024.07.039>.
- [38] M. Koehl, M. Heck, S. Wiesmeier, J. Wirth, Modeling of the nominal operating cell temperature based on outdoor weathering, *Sol. Energy Mater. Sol. Cells* 95 (2011) 1638–1646, <https://doi.org/10.1016/j.solmat.2011.01.020>.
- [39] J. Peng, L. Lu, H. Yang, T. Ma, Validation of the Sandia model with indoor and outdoor measurements for semi-transparent amorphous silicon PV modules, *Renew. Energy* 80 (2015) 316–323, <https://doi.org/10.1016/j.renene.2015.02.017>.
- [40] E. Skoplaki, A.G. Boudouvis, J.A. Palyvos, A simple correlation for the operating temperature of photovoltaic modules of arbitrary mounting, *Sol. Energy Mater. Sol. Cells* 92 (2008) 1393–1402, <https://doi.org/10.1016/j.solmat.2008.05.016>.
- [41] M. Akhasssi, A. El Fathi, N. Erraissi, N. Aarich, A. Bennouna, M. Raou, A. Outzourhit, Solar Energy Materials and Solar Cells Experimental investigation and modeling of the thermal behavior of a solar PV module 180 (2018) 271–279, <https://doi.org/10.1016/j.solmat.2017.06.052>.
- [42] A. Keddouda, R. Ihaddadene, A. Boukhari, A. Afia, M. Arici, N. Lebbihiat, N. Ihaddadene, Photovoltaic module temperature prediction using various machine learning algorithms: performance evaluation, *Appl. Energy* 363 (2024) 123064, <https://doi.org/10.1016/j.apenergy.2024.123064>.
- [43] L. Serrano-Luján, C. Toledo, J.M. Colmenar, J. Abad, A. Urbina, Accurate thermal prediction model for building-integrated photovoltaics systems using guided artificial intelligence algorithms, *Appl. Energy* 315 (2022) 119015, <https://doi.org/10.1016/j.apenergy.2022.119015>.

- [44] A. Keddouda, R. Ihaddadene, A. Boukhari, A. Atia, M. Arici, N. Lebbihiat, N. Ihaddadene, Experimentally validated thermal modeling for temperature prediction of photovoltaic modules under variable environmental conditions, Renew. Energy 231 (2024) 120922, <https://doi.org/10.1016/j.solener.2024.120922>.
- [45] S.F. Ahmed, M.S. Bin Alam, M. Hassan, M.R. Rozbu, T. Ishtiaq, N. Rafa, M. Mofijur, A.B.M. Shawkat Ali, A.H. Gandomi, Deep Learning Modelling Techniques: Current Progress, Applications, Advantages, and Challenges, Springer Netherlands, 2023, <https://doi.org/10.1007/s10462-023-10466-8>.
- [46] Y. Wu, B. Sicard, S.A. Gadsden, Physics-informed machine learning: a comprehensive review on applications in anomaly detection and condition monitoring, Expert Syst. Appl. 255 (2024) 124678, <https://doi.org/10.1016/j.eswa.2024.124678>.
- [47] T. Arcomano, I. Szunyogh, A. Wikner, J. Pathak, B.R. Hunt, E. Ott, A hybrid approach to atmospheric modeling that combines machine learning with a physics-based numerical model, J. Adv. Model. Earth Syst. 14 (2022) e2021MS002712, <https://doi.org/10.1029/2021MS002712>.
- [48] A. Quarteroni, P. Gervasio, F. Regazzoni, Combining physics-based and data-driven models: advancing the frontiers of research with Scientific, Mach. Learn. (2025) 1–127. <https://arxiv.org/abs/2501.18708>.
- [49] N. Martín-Chivelet, J. Polo, C. Sanz-Saiz, L.T. Núñez Benítez, M. Alonso-Abella, J. Cuenca, Assessment of PV module temperature models for building-integrated photovoltaics (BIPV), Sustain. Times 14 (2022) 1–15, <https://doi.org/10.3390/su14031500>.
- [50] G. Tina, F. Bontempo, L. Merlo, F. Bizzarri, Comparative analysis of monofacial and bifacial photovoltaic modules for floating power plants, Appl. Energy 281 (2021) 116084, <https://doi.org/10.1016/j.apenergy.2020.116084>.
- [51] A. Osama, G.M. Tina, A. Gagliano, Thermal models for mono/bifacial modules in ground/floating photovoltaic systems: a review, Renew. Sustain. Energy Rev. 216 (2025) 115627, <https://doi.org/10.1016/j.rser.2025.115627>.
- [52] M.B. Ogaard, V.S. Nysted, S. Rønneberg, G. Otnes, S.E. Foss, T. Mongstad, H. N. Riise, Vertical Bifacial PV Systems : Irradiance Modeling and Performance Analysis of a Lightweight System for Fl at Roofs, 2024, p. 13.
- [53] A.J. Carr, J. Liu, A. Binani, K. Cesar, B.B. Van Aken, Thermal model in digital twin of vertical PV system helps to explain unexpected yield gains, EPJ Photovoltaics 14 (2023), <https://doi.org/10.1051/epjp/2023027>.
- [54] R.A. Agathokleous, S.A. Kalogirou, Part I: thermal analysis of naturally ventilated BIPV system: experimental investigation and convective heat transfer coefficients estimation, Sol. Energy 169 (2018) 673–681, <https://doi.org/10.1016/j.solener.2018.02.048>.
- [55] M.A. Rahaman, T.L. Chambers, A. Fekih, G. Wiecheteck, G. Carranza, G.R. C. Possetti, Floating photovoltaic module temperature estimation: modeling and comparison, Renew. Energy 208 (2023) 162–180, <https://doi.org/10.1016/j.solene.2023.03.076>.
- [56] R.J.Y. Nebojsa Jakica, Mikkel Kragh, J.W.M. Pabasara, U. Wijeratne, Eric Too, Ron Wakefield, F.F. Eisenlohr, Simon Boddaert, Pierluigi Bonomo, Erika Saretta, J. L. Alessandra Zanelli, Sara Freitas, Philippe Alamy, BIPV. Design and Performance Modelling: Tools and Methods, 2019.
- [57] G.R. Venkatakrishnan, R. Rengaraj, S. Tamilselvi, J. Harshini, A. Sahoo, C. A. Saleel, M. Abbas, E. Cuce, C. Jazlyn, S. Shaik, P.M. Cuce, S. Riffat, Detection, location, and diagnosis of different faults in large solar PV system—a review, Int. J. Low Carbon Technol. 18 (2023) 659–674, <https://doi.org/10.1093/ijlct/ctad018>.
- [58] J. Kenfack, D. Kassegne, F. Menga, S.S. Ouro-djoko, Faults in a Photovoltaic System, 2023.
- [59] K. Osmanli, A. Haddad, T. Lemenand, B. Castanier, M. Alkhedher, M. Ramadan, A critical review of PV systems' faults with the relevant detection methods, Energy Nexus 12 (2023) 100257, <https://doi.org/10.1016/j.nexus.2023.100257>.
- [60] N. Ennemiri, A. Berrada, A. Emrani, J. Abdelmajid, R. El Mrabet, Optimization of an off-grid PV/biogas/battery hybrid energy system for electrification: a case study in a commercial platform in Morocco, Energy Convers. Manag. X 21 (2024) 100508, <https://doi.org/10.1016/j.ecmx.2023.100508>.
- [61] C.G. Lee, W.G. Shin, J.R. Lim, G.H. Kang, Y.C. Ju, H.M. Hwang, H.S. Chang, S. W. Ko, Analysis of electrical and thermal characteristics of PV array under mismatching conditions caused by partial shading and short circuit failure of bypass diodes, Energy 218 (2021) 119480, <https://doi.org/10.1016/j.energy.2020.119480>.
- [62] C. Zhang, Y. Zhang, J. Su, T. Gu, M. Yang, Modeling and prediction of PV module performance under different operating conditions based on power-law I-V model, IEEE J. Photovoltaics 10 (2020) 1816–1827, <https://doi.org/10.1109/JPHOTOV.2020.3016607>.
- [63] J. Kurnik, M. Jankovec, K. Brecl, M. Topic, Outdoor testing of PV module temperature and performance under different mounting and operational conditions, Sol. Energy Mater. Sol. Cells 95 (2011) 373–376, <https://doi.org/10.1016/j.solmat.2010.04.022>.
- [64] G. Ciulla, V. Lo Brano, V. Franzitta, M. Trapanese, Assessment of the operating temperature of crystalline PV modules based on real use conditions, Int. J. Photoenergy 2014 (2014), <https://doi.org/10.1155/2014/718315>.
- [65] International Energy Agency, World Energy Outlook (2022), [https://www.iea.org/reports/world-energy-outlook-2022?utm\\_source=SendGrid&utm\\_medium=E-mail&utm\\_campaign=IEA+newsletters](https://www.iea.org/reports/world-energy-outlook-2022?utm_source=SendGrid&utm_medium=E-mail&utm_campaign=IEA+newsletters).
- [66] M. Perez, R. Perez, K.R. Rábago, M. Putnam, Overbuilding & curtailment: the cost-effective enablers of firm PV generation, Sol. Energy 180 (2019) 412–422, <https://doi.org/10.1016/j.solener.2018.12.074>.
- [67] M.J. Perez, R. Perez, T.E. Hoff, Ultra-high photovoltaic penetration: where to deploy, Sol. Energy 224 (2021) 1079–1098, <https://doi.org/10.1016/j.solener.2021.06.041>.
- [68] M. Pierro, R. Perez, M. Perez, M.G. Prina, D. Moser, C. Cornaro, Italian protocol for massive solar integration: from solar imbalance regulation to firm 24/365 solar generation, Renew. Energy 169 (2021) 425–436, <https://doi.org/10.1016/j.solener.2021.01.023>.
- [69] W. Herrmann, G. Eder, B. Farnung, G. Friesen, M. Köntges, B. Kubicek, O. Kunz, H. Liu, D. Parlevliet, I. Tsanakas, IEA-PVPS task 13: performance, operation and reliability of photovoltaic systems—qualification of photovoltaic (PV) power plants using mobile test equipment, Report, Int. Energy Agency (2021).
- [70] G. Jiménez-Castillo, F.J. Muñoz-Rodríguez, C. Rus-Casas, P. Gómez-Vidal, Improvements in performance analysis of photovoltaic systems: array power monitoring in pulse width modulation charge controllers, Sensors (Switzerland) 19 (2019), <https://doi.org/10.3390/s19092150>.
- [71] G. Jiménez-Castillo, F.J. Muñoz-Rodríguez, C. Rus-Casas, J.C. Hernández, G. M. Tina, Monitoring PWM signals in stand-alone photovoltaic systems, Meas. J. Int. Meas. Confed. 134 (2019) 412–425, <https://doi.org/10.1016/j.measurement.2018.10.075>.
- [72] O.C. Akinsipe, D. Moya, P. Kaparaju, Design and economic analysis of off-grid solar PV system in Jos-Nigeria, J. Clean. Prod. 287 (2021) 125055, <https://doi.org/10.1016/j.jclepro.2020.125055>.
- [73] A.K.B.A.R. Satria Putra, H.A.S.T.I. Afianti, R.I.C.H.A. Watiasih, COMPARATIVE ANALYSIS OF SOLAR CHARGE CONTROLLER PERFORMANCE BETWEEN MPPT AND PWM, J. Electr. Eng. Comput. Sci. 7 (2022) 1197–1202.
- [74] M. Waqar Akram, G. Li, Y. Jin, X. Chen, Failures of photovoltaic modules and their detection: a review, Appl. Energy 313 (2022) 118822, <https://doi.org/10.1016/j.apenergy.2022.118822>.
- [75] E. Ogliari, A. Dolara, D. Mazzeo, G. Manzolini, S. Leva, Bifacial and monofacial PV systems performance assessment based on IEC 61724-1 standard, IEEE J. Photovoltaics 13 (2023) 756–763, <https://doi.org/10.1109/JPHOTOV.2023.3295869>.
- [76] I. Jahn, Ulrike, Herz, Magnus, Köntges, Marc, Parlevliet, David, Paggi, Marco, Tsanakas, Review on Infrared and Electroluminescence Imaging for PV Field Applications: International Energy Agency Photovoltaic Power Systems Programme, 2018. IEA PVPS Task 13, Subtask 3.3: report IEA-PVPS T13-12: 2018.
- [77] H. Ahn, D. Rim, G.S. Pavlak, J.D. Freihaut, Uncertainty analysis of energy and economic performances of hybrid solar photovoltaic and combined cooling, heating, and power (CCHP + PV) systems using a Monte-Carlo method, Appl. Energy 255 (2019) 113753, <https://doi.org/10.1016/j.apenergy.2019.113753>.
- [78] M. Bardhi, G. Grandi, G.M. Tina, Comparison of PV cell temperature estimation by different thermal power exchange calculation methods, Renew. Energy Power Qual. J. 1 (2012) 653–658, <https://doi.org/10.24084/repqj10.417>.
- [79] G. Mannino, G.M. Tina, G. Jiménez-Castillo, M. Cacciato, F. Bizzarri, A. Canino, Nonlinear and multivariate regression models of current and voltage at maximum power point of bifacial photovoltaic strings, Sol. Energy 269 (2024), <https://doi.org/10.1016/j.solener.2024.112357>.
- [80] A. Idzkowski, K. Karasowska, W. Walendziuk, Temperature analysis of the stand-alone and building integrated photovoltaic systems based on simulation and measurement data, Energies 13 (2020), <https://doi.org/10.3390/en13164274>.
- [81] T.A. Olukan, M. Emziane, A comparative analysis of PV module temperature models, Energy Prog. 62 (2014) 694–703, <https://doi.org/10.1016/j.egypro.2014.12.433>.
- [82] IEC/TS 61836, Solar Photovoltaic Energy Systems – Terms, Definitions and Symbols, 2007.
- [83] PVsyst, PVsyst-NOCT Definition, (n.d.). [https://www.pvsyst.com/help/index.html?noct\\_definition.htm](https://www.pvsyst.com/help/index.html?noct_definition.htm).
- [84] IEC, IEC TS 61724-2:Photovoltaic system performance – Part 2: capacity evaluation method. <https://solargostaran.com/files/standards/IEC/IECTS61724-2-2016.pdf>, 2016.
- [85] A. Keddouda, R. Ihaddadene, A. Boukhari, A. Atia, Experimental and numerical modeling of photovoltaic modules temperature under varying ambient conditions, Energy Convers. Manag. 312 (2024) 118563, <https://doi.org/10.1016/j.enconman.2024.118563>.
- [86] D. Faiman, Assessing the outdoor operating temperature of photovoltaic modules, Prog. Photovoltaics Res. Appl. 16 (2008) 307–315, <https://doi.org/10.1002/pip.813>.
- [87] C.C. Smith, T.A. Weiss, Design application of the Hottel-Whillier-Bliss equation, Sol. Energy 19 (1977) 109–113, [https://doi.org/10.1016/0038-092X\(77\)90047-0](https://doi.org/10.1016/0038-092X(77)90047-0).
- [88] A. Driesse, M. Theristis, J.S. Stein, PV module operating temperature model equivalence and parameter translation, Conf. Rec. IEEE Photovolt. Spec. Conf. (2022) 172–177, <https://doi.org/10.1109/PVSC48317.2022.9938895>, June (2022).
- [89] F.P. Arrays, A Simplified Thermal Model for Flat-Plate Photovoltaic Array, 1987.
- [90] M. Zouine, M. Akhsassi, N. Erraissi, N. Aarich, A. Bennouna, M. Raoufi, A. Outzourhit, Mathematical models calculating PV module temperature using weather data: experimental study, Lect. Notes Electr. Eng. 519 (2019) 630–639, [https://doi.org/10.1007/978-981-13-1405-6\\_72](https://doi.org/10.1007/978-981-13-1405-6_72).
- [91] R.G. Ross Jr., M.I. Smokler, Electricity from photovoltaic solar cells: flat-Plate Solar array project final report. Volume VI: engineering sciences and reliability, jet propuls, Lab (1986) 1–98. <https://resolver.caltech.edu/CaltechAUTHORS:JPLpub86-31-volumeVI>.
- [92] E. Skoplaki, J.A. Palyvios, Operating temperature of photovoltaic modules: a survey of pertinent correlations, Renew. Energy 34 (2009) 23–29, <https://doi.org/10.1016/j.renene.2008.04.009>.
- [93] W.A. Beckman Duffie, Solar Engineering of Thermal Processes, second ed., John Wiley and Sons, New York, 1991.
- [94] A.Q. Jakhrani, A.K. Othman, A.R.H. Rigit, S.R. Samo, Determination and comparison of different photovoltaic module temperature models for Kuching,

- Sarawak, 2011 IEEE 1st Conf, Clean Energy Technol. CET 2011 (2011) 231–236, <https://doi.org/10.1109/CET.2011.6041469>.
- [95] H. Oufettou, N. Lamdihine, S. Motahhir, N. Lamrini, I.A. Abdelmoula, G. Aniba, Comparative performance analysis of PV module positions in a solar PV array under partial shading conditions, *IEEE Access* 11 (2023) 12176–12194, <https://doi.org/10.1109/ACCESS.2023.3237250>.
- [96] N. Manoj Kumar, S. Chakraborty, S. Kumar Yadav, J. Singh, S.S. Chopra, Advancing simulation tools specific to floating solar photovoltaic systems – comparative analysis of field-measured and simulated energy performance, *Sustain. Energy Technol. Assessments* 52 (2022) 102168, <https://doi.org/10.1016/j.seta.2022.102168>.
- [97] Y. Chaibi, A. Allouhi, M. Malvoni, M. Salhi, R. Saadani, Solar irradiance and temperature influence on the photovoltaic cell equivalent-circuit models, *Sol. Energy* 188 (2019) 1102–1110, <https://doi.org/10.1016/j.solener.2019.07.005>.